NASA TECHNICAL MEMORANDUM NASA TM-76275

DEVELOPMENT OF A FEED MONITOR SYSTEM FOR A HELIUM-COOLED MICHELSON INTERFEROMETER FOR THE SPACELAB

P. Essenwanger

(NASA-TM-76275) DEVELOPMENT OF A FEED MONITOR SYSTEM FOR A HELIUM-COOLED MICHELSON INTERFEROMETER FOR THE SPACELAB (National Aeronautics and Space Administration) 75 p HC A04/MF A01 CSCL 14B G3/35

N80-26642

Unclas 27976

Translation of "Entwicklung eines Vorschubmesssystems fuer ein heliumgekuehltes Michelsoninterferometer auf Spacelab," Max-Planck-Institut fuer Physik und Astrophysik, Institute for Extraterrestrial Physics, Garching bei Muenchen, West Germany, Report MPI-PAE/Extraterr. 161, January 1980, pp 1-85

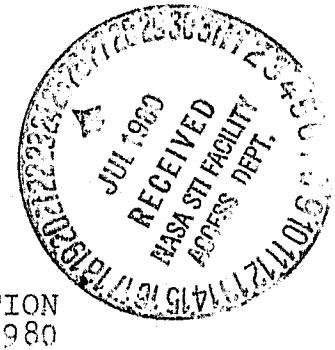

NATIONAL AERONAUTICS AND SPACE ADMINISTRATION
WASHINGTON, D.C. JUNE 1980

STANDARD TITLE PAGE

1. Report No.	2. Government Accession No.	3. Recipient's Catalog No.
NASA TM-76275		

4. Title and Subtitle	5. Report Date
DEVELOPMENT OF A FEED MONITOR SYSTEM FOR A HELIUM-COOLED MICHELSON INTERFEROMETER FOR THE SPACELAB	June 1980
	6. Performing Organization Code
7. Author(s)	8. Performing Organization Report No.
Peter Essenwanger	10. Work Unit No.
9. Performing Organization Name and Address	11. Contract or Grant No.
Leo Kanner Associates Redwood City, California 94063	NASW-3199
	13. Type of Report and Period Covered
12. Sponsoring Agency Name and Address	Translation
National Aeronautics and Space Administration, Washington, D.C. 20546	14. Sponsoring Agency Code

15. Supplementary Notes

Translation of "Entwicklung eines Vorschubmesssystems fuer ein heliumgekuehltes Michelsoninterferometer aur Spacelab," Max-Planck-Institut fuer Physik und Astrophysik, Institut for Extraterrestrial Physics, Garching bei Muenchen, West Germany, Report MPI-PAE/Extraterr. 161, January 1980, pp 1-85

16. Abstract

A Michelson interferometer feed monitor system developed for Spacelab is described. The device is helium cooled and will be used to measure far infrared radiation sources in space. Performance data and development sequence are presented.

17. Key Words (Selected by Author(s))	18. Distribution Statement
	Unclassified Unlimited

19. Security Classif. (of this report)	20. Security Classif. (of this page)	21. No. of Pages	22. Price
Unclassified	Unclassified	75	

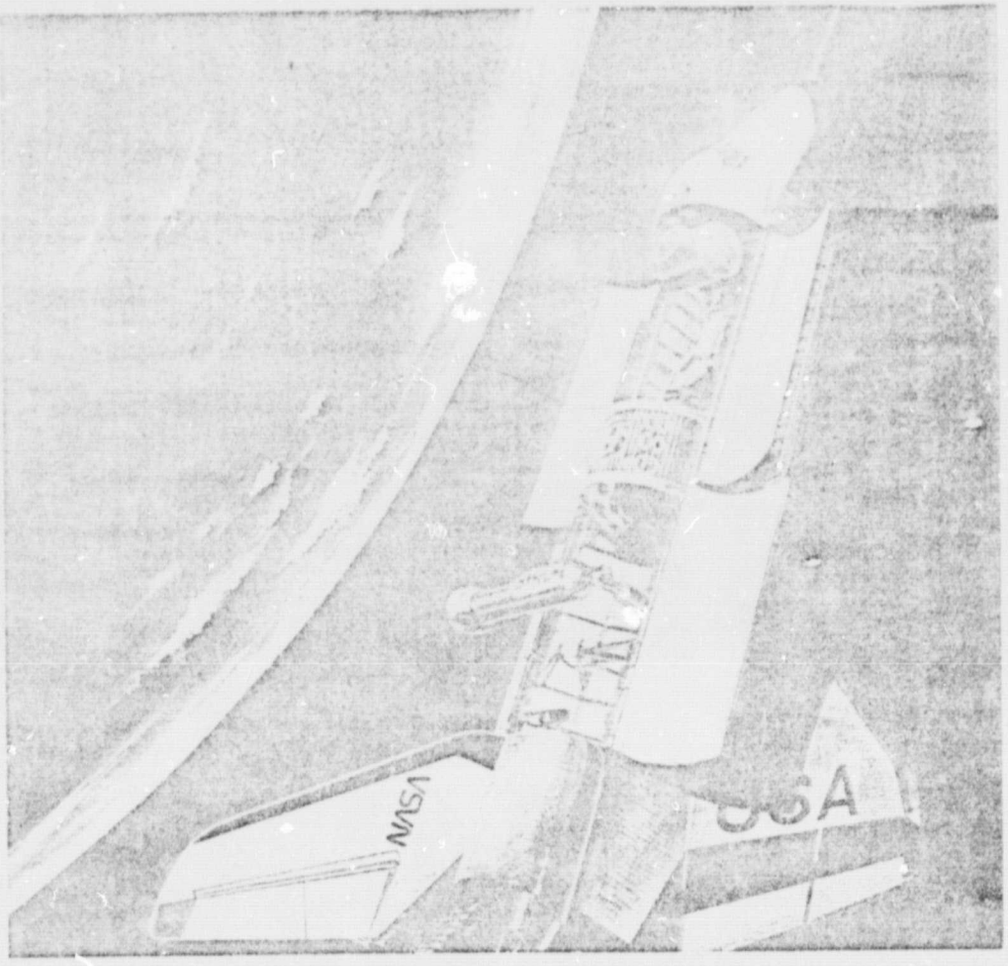

The GIRL infrared telescope will perform observations from spacelab in 1984.

Table of Contents

DEVELOPMENT OF A SPEED MONITOR SYSTEM FOR A HELIUM-COOLED MICHELSON INTERFEROMETER FOR THE SPACELAB

P. Essenwanger

1. Introduction

1.1 Astronomy in the Far Infrared

Due to the development of high sensitivity detectors and advancements in cryotechniques, the entire infrared spectral range has been made accessible to astronomy within the last decade. Astronomical observations in the far infrared (FIR) provide important information for explaining fundamental questions of Astrophysics. Contributions to an understanding of the dynamics of the galaxy are expected. Particularly on the question of the connection between the stars and the interstellar medium (formation and destruction of stars, star generation rate). A large fraction of the cosmic objects to be investigated are particularly suitable for observation in the far infrared (20 μm to 800 μm): /1*

a) Cold objects (temperature several K to several 100 K) like prostellar clouds emit the majority of radiation energy in this spectral range.

b) The radiation emitted from hot objects ($T \gtrsim 1000$ K) like gas clouds and galactic nuclei at greater distances from the sun (>1 kpc) primarily in the visible and UV spectral range is greatly weakened by the wavelength dependent dust extinction, whereas FIR radiation passes through.

c) In dense clouds, molecules (especially H_2) which cannot be observed by radio transmission because of their small or absent dipole moment can be detected by FIR.

After these successes of Photometry in the last decade, the high information content of line radiation (for derivation of temperature, density, element frequency, degree of ionization, electron density) has been opened up by spectroscopy. These measurements allow decisive improvements in the model for the general interstellar medium or for planetary mist. The low development status of IR technology (IR detectors, cryotechnology) and the strong absorption and emission of water vapor in the earth's atmosphere have hindered earlier spectroscopic investigations. Through the use of IR telescopes on balloons or satellites, extensive observations are possible, whereby at balloon heights ($\sim$ 50 km) the emission of the residual atmosphere still severely reduces the sensitivity of the measurements. Another inter- /2

*Numbers in the margin indicate pagination in the foreign text.

fering factor is the thermal emission of the telescope. However, this can be reduced so much by cooling that at satellite altitudes the advantage of low environmental radiation can be fully utilized. Thus, the necessary high sensitivity of the instrument is achieved (the emission power output at the detector of a 1-m-telescope is on the range of 10^{-15} W per spectral line).

1.2 The Michelson Interferometer Based on GIRL

As the first helium-cooled telescope for satellite observations also performing FIR spectroscopy, the German Infra-Red Laboratory (GIRL) is now under construction. Its employment on Spacelab is intended for 1984. Behind the 40 cm telescope (relative opening ratio f/10) are four instruments for astronomy and cosmonomy. A 300 liter tank with supercooled helium is in good thermal contact with the instruments and telescope which is to have a temperature of $\approx$ 10 K in space observation.

The objective of GIRL is primarily the observation of star generation regions in the far reaches of the Milky Way and of galaxies. The following instruments will be used: a IR camera, a Photometer/Polarimeter, a Ebert-Fastie spectrometer of moderate resolution (which is to perform measurements of the emissions of the earth's atmosphere), and a Michelson interferometer for high resolution spectroscopy in the far infrared (Lemke et al. 1979). This instument is being developed at the Institute for Extraterrestrial Physics. It is intended for spectroscopic use in the range of 20 μm - 200 μm with a spectral resolution of (0.03/cm) on the order of the widths of the measured lines. Figure 1 shows the design of the Michelson interferometer. First, the beam path of the astronomic radiation is described. It moves through an tuning lens into the focal plane of the instrument. A parallel beam bundle of about 4 cm diameter is generated by a Off-Axis-Paraboloid. This bundle is split at the beam splitter to the two interferometer arms and the twin partial beams are reunited after reflection from two plane mirrors at the beam splitter. (Use of /3
a cube horner is discussed below.) A second parabolic mirror focuses the beam bundle onto the detector. By using a suitable, high sensitive detector (NEP < 10^{-16} W/ [illegible], radiation power outputs of < 10^{-16} W per spectral line at an integration time of about 100 seconds can be detected. Thus, the detection limit of the system (determined by the interference radiation at a Etendue $2 \cdot 10^3$ cm^{2}sr) is practically attained.

To adapt the beam path to the space relationships in the GIRL /4
cryostat, the beam is diverted several times. The partial beam of the mobile interferometer arm is sent through a cube corner (three plane mirros perpendicular to each other) which can be moved on a roll table. In this manner the cube corner can be shifted by 10 cm to achieve an optimum path difference of L = 40 cm. The fact that tip motions of the cube corner of about 1 degree do not result in misadjustment of the partial beam is of great significance. The drive of the roll table on which the cube corner is found, is performed by a crankless engine. The time change of optical path length is 400 μm/sec--determined by the maximum permissible observation time (mission requirements). The useful spectral range is determined by the wavelength dependent effectiveness of the beam splitter (mylar foil) and

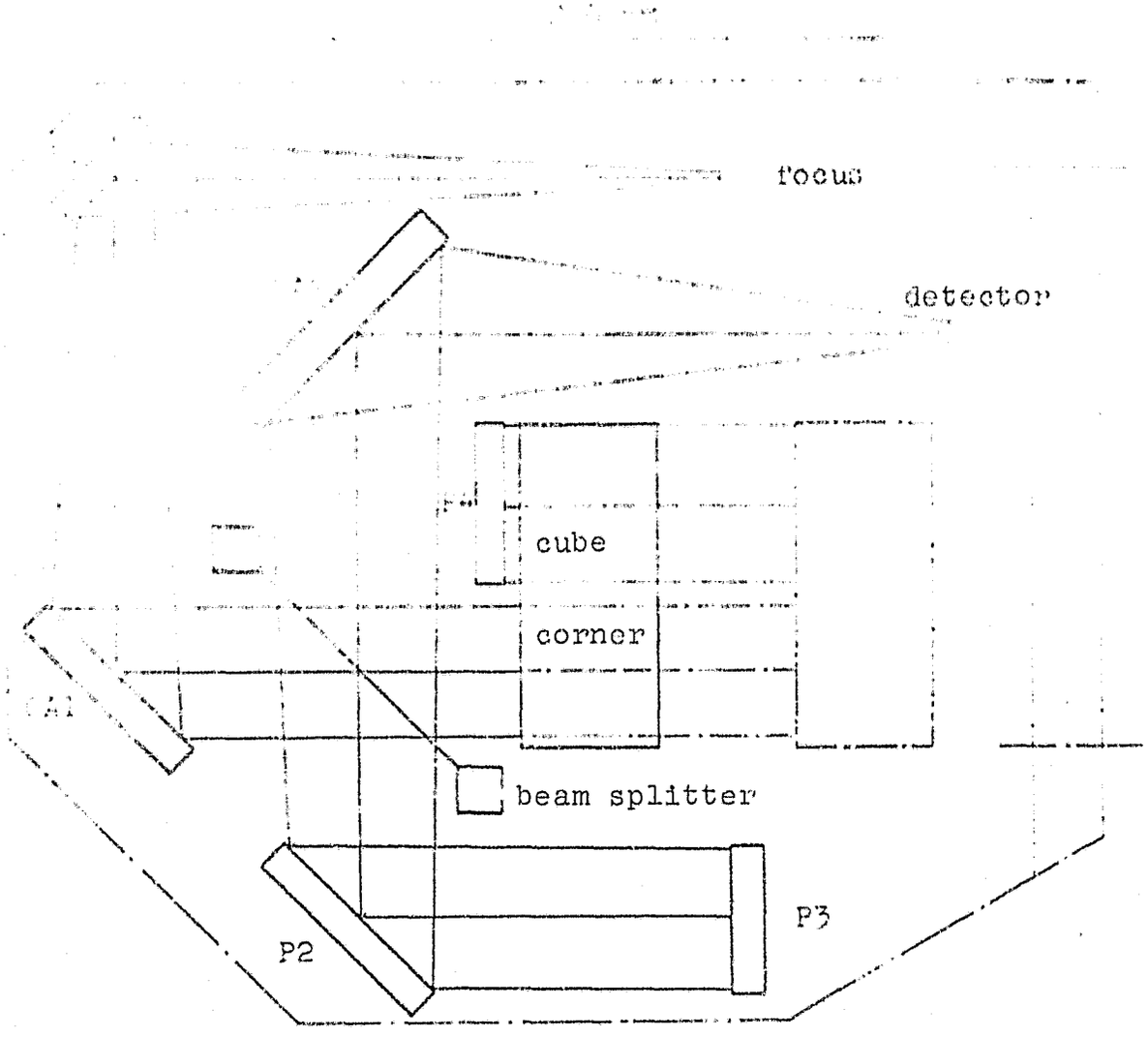

P: Plane mirror
OA: Off-Axis Paraboloid

Figure 1: Beam path of the Michelson interferometer for GIRL

the spectral sensitivity range of the detector. All components of the inferometer are located in a high vacuum and cooled to helium temperature.

1.3 Evaluation of the Interferogram

As is known, interference between the two partial beams whose phase difference is changed continually by shifting cube corner leads to an intensity modulation at the detector. The intensity I of the radiation or of the corresponding detector signal S as a function of the optic path difference x is called the interferogram. The spectrum of observed radiation (intensity B as a function of wave number $\tilde{\nu}$)

follows from the interferogram by Fourier transformation:

(1.1)

From the limited nature of the optical path difference ( ) there results errors in the spectrum which can be partially corrected by apodization. Without this correction we obtain the following equation for the spectral resolution as a function of the maximum path difference L (see for instance Vanasse, Saka 1971):

(1.2)

From this there results for the GIRL Michelson interferometer = 0.013 cm^{-1}. /5

The program controlled evaluation of the interferogram is implemented by a time saving FFT Algorithm (e.g. Cooley-Tukey). It is necessary to measure the interferogram values at equidistant support points. In order not to deteriorate the resolution given by equation 1.2 in the useful spectral range with the upper and lower boundary wave numbers $_2$ or $_1$, the support points must be valid for the minimum number N_0 (Sampling-Theorem):

(1.3)

A deviation from the actual path differences from the support points used to evaluate the interferogram results in errors in the spectrum. The feed monitor system provides an assignation between the interferogram values and the attendant optical path differences. It is thus of critical importance that the accuracy of measurement also determines the quality of the spectrum.

The objective of this work was to develop a new feed monitor system which satisfies the requirements of low operating temperatures in order to use it for the cooled Michelson interferometer on GIRL. Its function consists in a highly accurate measurement of the distances to the support points.

2. Principle Description of the Feed Monitor System /6

In this section the accuracy of feed monitoring will be derived from the Fourier spectrum[1] (Section 2.1). From this results the necessity for an interferometer system to measure the optical path difference (determination of position of the cube corner). The conception of this system is described in detail in Section 2.2.

2.1 Derivation of Measurement Accuracy of the Feed Monitor System

Initially, the relationships between the location accuracy of support points and the quality of the Fourier spectra will be studied.

---

[1] In order to avoid confusion, the interferogram of the radiation determined from the observed objects is called the main interferogram below, and the spectrum obtained from Fourier transformation is called the Fourier spectrum.

If the data on support point position is affected by errors, then upon transformation we obtain an artificial noise in the spectrum. Proceeding from the case of a periodic error in the determination of support point position, the influence of a corresponding random (statistic) error is derived.

The actual optical path difference x' where the readout of the main interferometer occurs (readout position), differs generally from the measured path difference x (support point) which is assigned to the readout value S upon transformation of the interferogram S(x). The difference Δx:

$$\Delta x = x' - x \tag{2.1}$$

is called the support point error. A sine shaped error of amplitude "a" and period length P is given by:

$$\Delta x = a \sin \frac{2\pi}{P} x \tag{2.2}$$

and generates numerous ghost lines with wave numbers $\sigma = \sigma_F \pm \frac{n}{P}$, $n = 1 \ldots N$ in the Fourier spectrum in the vicinity of a genuine spectral line (wave number σ_F). For small products of wave number and error amplitude, only the line pair with n = 1 is of importance. According to Saka (1970), Parsche (1973), it posesses the relative peak height--measured by the level of the actual spectral line: /7

$$\beta = \pi \sigma_F a \qquad \text{for } \beta = \pi \sigma_F a < 1 \tag{2.3}$$

and the spectral interval $\Delta\sigma_F = \pm \frac{1}{P}$. Overall, the line spectrum consists of line tripletts and only the middle line is a real spectral line.

A statistically distributed support point error can be attributed to the periodic case through Fourier analysis (Appendix 1). Numerous ghost lines appear in the Fourier spectrum. The relative peak $\bar{\beta}$--qradratically determined via the spectral elements--can be determined from the standard deviation of support points σ_x:

$$\bar{\beta} = \pi \sigma_F \sigma_x \tag{2.4}$$

They result in errors in determination of intensities of real spectral lines. For an average peak height B they obtain a standard deviation of line intensities:

$$\sigma_B = B \cdot \bar{\beta} . \tag{2.5}$$

Thus the Fourier spectrum is superimposed by noise which comes into being nearly through transformation of the interferogram with an erroneously measured support point. The S/N ratio accordingly is:

$$\frac{B}{\sigma_B} = \frac{1}{\pi \sigma_F \sigma_x} \tag{2.6}$$

For the Fourier spectra of the GIRL interferometer, a S/N ratio

of 100 is desired (dynamic range). From equation 2.6 we thus obtain the corresponding requirement of measurement accuracy when using the maximum wave number in the useful spectral range (= 500 cm-1 = 20 μm) as . . . This high local resolution is generally not achieved by feed monitor systems based on mechanical principles. Interferometric length measurements cannot satisfy these requirements. Therefore, use of a position interferometer is provided here; this design will be described in the following section. /8

2.2 Description of the Position Interferometer

The position interferometer consists primarily of the main interferometer and several additional components: the main beam path of the GIRL interferometer is also used, a monochromatic emission source and a radiation detector is also installed (see Figure 2).

The primary difficulties in the design of the position interferometer are the extreme operating conditions on GIRL (helium temperature and high vacuum). For the first time, a helium cooled semiconductor diode laser in the near IR range will be used as a monochromatic reference emission source. The laser beam is converted into a parallel bundle by a suitable lens which utilizes the primary beam path. This reference beam generates an interferogram recorded by the auxiliary helium cooled detector. Simultaneously, readout of the primary interferogram by the main detector takes place. Measurement of the optical path difference does not occur through counting off the intensity maxima or minima in the laser interferogram, but through accurate reading of the intensity profile at the appropriate detector. Through evaluation of this position interferogram a complicated electronic system is needed whose concept and mode of operation are described in Appendix 2. The variable term (cosine term) S_L of the interferometer signal at the detector output is decisive here; for constant chronological change of optical path difference with the optical feed velocity v, this term has the form:

(2.7)

Here, S_o is the amplitude of the signal and $\tilde{\nu}_L$ the laser wave number used . . . The signal frequency is 80 Hz at the intended values (v = 400 μm/sec), the periodicity is T= 1/f = 12.5 msec. Processing of the signal takes place digitally in time increments of τ = T/128 (integration time) and voltage steps of u = 2.44 mV. At the extremal and zero points of the signal S_L the position electronic system gives off pulses which trigger the readout of the main interferogram. A readout pulse is generated at the first recognizable drop in the signal at a relative extreme and for so-called zero passage of the signal (i.e. the signal exceeds or falls below the arithmetic average of the last maximum and minimum value, Figure 3). The extremal and zero points thus mark the ideal equidistant support points for the Fourier transformation. When using all extremes and zero passages we obtain a total of $4L/\lambda_L$ = 320,000 support points, i.e. greater by a factor of nine than necessary for the spectral resolution (9 fold over sampling; /10

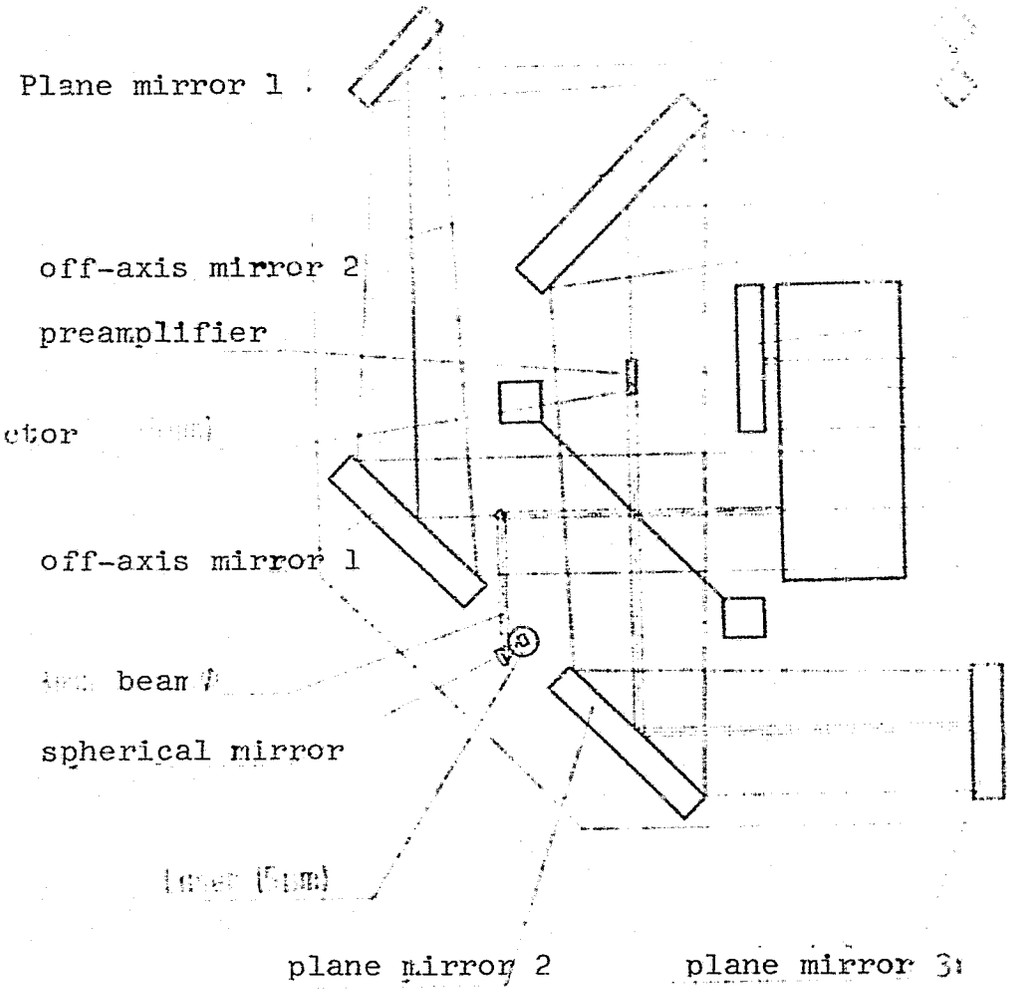

Figure 2: Beam path of the GIRL interferometer. In addition, beam path (3 mm beam diameter) and specific components (laser 5 μm, detector 5 μm) of the feed monitor system are illustrated.

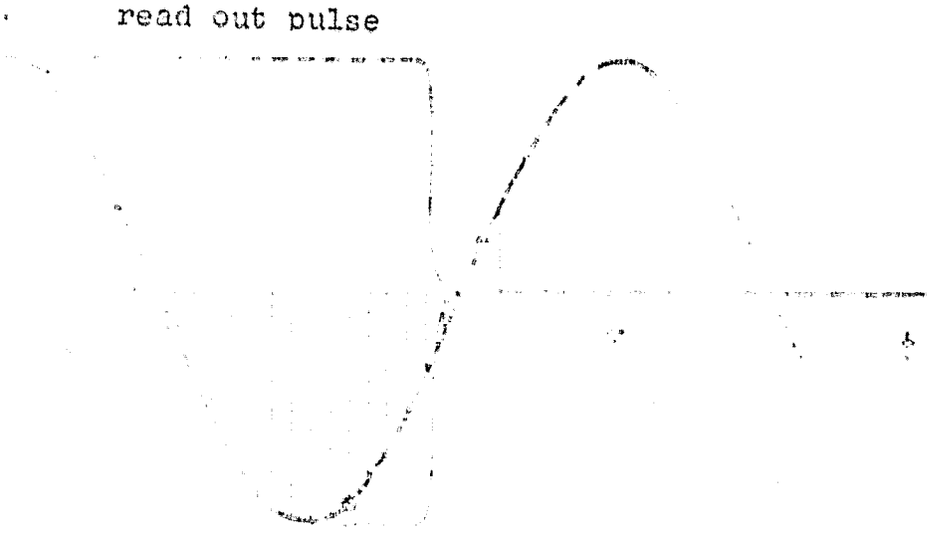

Figure 3: Schematic illustration of the readout of the interferometer signal $S_L(t)$. Integration time $\tau = 10^{-4}$ at T = 12.5 msec. M_o: arithmetic average of the maximum and subsequent minimum value.

see Equation 1.3). In itself, a laser of longer wavelength could be used to obtain a sufficient number of support points (maximal λ_L = 44 μm), however its exact positioning can no longer be determined with the needed accuracy.

Interference with the signal can change the readout position and generate additional relative extremes which lead to false pulses. Below, the deviation in pulse position from the position of the ideal support points--local resolution of position electronic system--caused by the positioning electronic system is studied. For an undisturbed interferometer signal S_L the resolution is limited by the duration of integration time τ. For a shift Δx compared to the ideal position we have: /11

$$\Delta x = v\tau = \frac{\lambda_L}{12} = 3.7 \ \mu m \qquad (2.8)$$

The minimum voltage recognized by the position electronic system is u = 2.44 mV. If the signal is measured at the maximum, then the measured value offset by τ is $\Delta S = S_o - S_L(\tau)$ below the maximum value S_o; [illegible] Equation 2.7 we obtain for an amplitude $S_o \approx 1.9$ V a drop of [illegible], which is recognized. If the measurement (in the worst case) is performed to the right and left of the maximum (see Figure 3), then the signal change is $\Delta S = 0$ and the electronic system does not react until the next time increment. The result is an inaccuracy in the position of the pulse of $\pm$ 0.02 μm at the extremal position. This results from a similar discussion of the zero passage. When using the equivalent support point (extremal position or zero position) we also obtain an average constant shift of [illegible] (extrema) or [illegible] μm (zero passages), which has no effect upon transformation

of the main interferogram and is thus of no importance. If the amplitude S_o drops below the minimum permissible input voltage U_{min} = 1.9 V, then the recognition of the extrema is delayed even more.

The noise superimposed on the signal results in fluctuations in discreet signal values. Corresponding to an integration time of $\tau = 10^{-4}$ sec, the effective noise bandwidth is 10^4 Hz. The noise voltage N can be estimated from the requirement: . . Thus, for the minimum permissible S/N ratio S_o/N in the interferogram we have the following equation for the minimum amplitude (S_o = 1.9 V): /12

(2.9)

This value must be maintained by the detection system in order to assure precise signal processing. By reducing the integration time τ and a corresponding drop in the noise level (see equation 2.9), these support point errors can be reduced.

The existing position electronic system was constructed by electricians at the institute. Tests under various boundary conditions are described in Section 4.4.

3. Derivation of Requirements of the Main Components of the Feed Monitoring System /13

The requirements of the most important components of the feed monitoring system, namely the reference beam source (laser), the assigned detector and beam splitter are derived in the following sections.

3.1 Requirements of the Semiconductor Diode Laser

The important properties which the diode laser used as a reference radiation source must have, are spectral purity and wavelength constancy. These are treated in the following sections. The radiation power is important primarily in connection with the detector (see Section 3.2). From the mission requirements there result additional secondary conditions like the maintenance of a loss power of about 200 mW (with respect to the coolant consumption). These and similar requirements are checked experimentally in Section 4.1.

3.1.1 The Spectral Intensity Distribution

In this section we examine how deviations in the reference beam from monochromatic radiation affect the laser interferogram and how the position of the support points can be thereby affected. The width of the laser line and additional occurring secondary lines must be considered. The spectral properties must be brought into harmony with the requirements presented in Section 2.

a) Effects of Line Width

The emission lines from diode lasers have Lorentz-like line profiles

because of the line propagation processes (Hempstead, Lax 1967) measured by Heterodyn spectroscopy by Hinkley, Freed (1969). The interferogram of a corresponding spectral line of average frequency ν_I and 3 db bandwidth 2ϵ is:

(3.1)

and it has the form (Dowling 1970): /14

(3.2)

(Figure 4). The amplitude of the interferogram decreases exponentially which can result in an inhibition of the evaluation of the extremal point through the position electronic system. In order to retain uniform accuracy of support points during the measurement process, a reduction in amplitude from $U_0 = 5V$ to a value below $U_{min} = 1.9$ V (see Section 2.2) should be prevented. For a typical line width of the IR diode laser of $\epsilon = 3.10^{-4}$/cm a retreat of the amplitude to 4.6 V is expected and this has no effect on the location resolution.

The exponential behavior of the envelopes of I(x) leads to an additional affect on local resolution as a result of the shift in extremal position. By Differentiation of equation 3.2 we obtain the condition for the new extremal position x':

(3.3)

From this results the constant shift Δx of the extremal position compared to the values of the ideal case as:

(3.4) /15

The zero positions of the top interferogram (Equation 3.2) are not shifted, however the arithmetic average from maximum value and subsequent minimum value are different from zero. This also leads to a shift in zero passages of (Appendix 3):

(3.5)

This shift in support points compared to the ideal positions for monochromatic radiation (equation 3.4, 3.5) is proportional to the line width. For typical line widths the support point error is only a few 10^{-7} μm, so that these effects are of no practical significance.

b) Effects of Secondary Lines

Diode lasers generally emit radiation at several frequencies, the appearance of secondary lines in addition to the high power primary line is normal. From this results severe differences in the laser interferogram whose effect on the support point position may differ. Initially, the case of an additional line (wavelength λ_N,

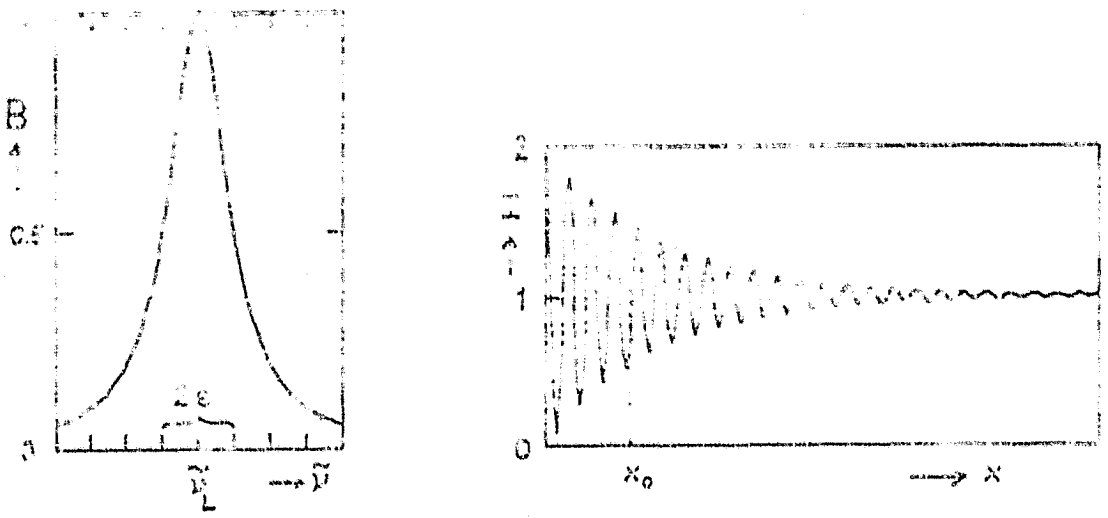

Figure 4: Graphic illustration of a laser line and its interferograph I(x). Typical values are $\epsilon = 3.10^{-4}$ cm^{-1}, optical path difference x_o=3.7 m.

interferogram amplitude S_1) beside the primary line (wavelength λ_L, amplitude S_o) will be considered by neglecting the line widths. The attendant interferometer signal is obtained in a similar manner by superposition of the individual signals $S_L(x) = S_o \cos 2\pi\tilde{\nu}_L x$ and $S_N(x) = S_1 \cos 2\pi\tilde{\nu}_N x$. as:

$$S(x) = S_o \cos 2\pi\tilde{\nu}_L x + S_1 \cos 2\pi\tilde{\nu}_N x \; . \qquad (3.6)$$

Figure 5 is an illustration of the appropriate example. The zero positions and extrema of S are shifted compared to the ideal support points of the unaffected signal S_L. Calculation of the shift for the zero positions (see Appendix 4) gives approximately the following equation for small amplitude ratios S_1/S_o with $\Delta\tilde{\nu} = \tilde{\nu}_L - \tilde{\nu}_N$:

$$\Delta x = \frac{\lambda_L}{\pi} \frac{S_1}{S_o} \sin 2\pi\Delta\tilde{\nu} x \; . \qquad (3.7)$$

We are dealing here with a periodic error of amplitude . /16

For more intense secondary lines, deviations from the sinusoidal form appear, whereby the location dependence is now very complicated and for the amplitude we have (Appendix 4):

(3.8)

Figure 5: Example for interferograph S of twin emission lines caused by superimposition of the individual interferograph S_L and S_N: $S_o = 1$, $\tilde{\nu}_L = 1500/cm$, $S_1 = 0.5$), ($\tilde{\nu}_N = 1700/cm$) (equation 3.6). The perpendicular lines mark the ideal positions of the zero points given by the undisturbed signal S_L.

To investigate the shifts of the extremal positions and of the zero passages and to consider the effects of several lines, numeric calculations are used (Wilczek 1979). It turns out that the distance of the laser lines has a minor influence on the support point position. For typical line separations (ca. 2/cm, see Section 4.1.2), this effect is hardly noticed. The numerically determined support point errors (deviations of extrema and zero passages) agree in the case of a secondary line with the analytically determined errors of zero points. The presence of several secondary lines leads to larger support point errors. The sinusoidal errors of each secondary line /17
are superimposed on each other whereby--regardless of the number of lines--an approximately linear relation exists between the maximum error and the total intensity of the secondary lines. Figure 6 shows the dependence of the error amplitude on the intensity ratio S_1/S_o of the secondary and primary line using the example of one and three secondary lines for $\tilde{\nu}_L = 2000/cm$. The periodic support point error of a secondary line generates line triplets in the Fourier spectrum during a Fourier transformation. For the relative level of ghost lines in the vicinity of the spectral line of the astronomic

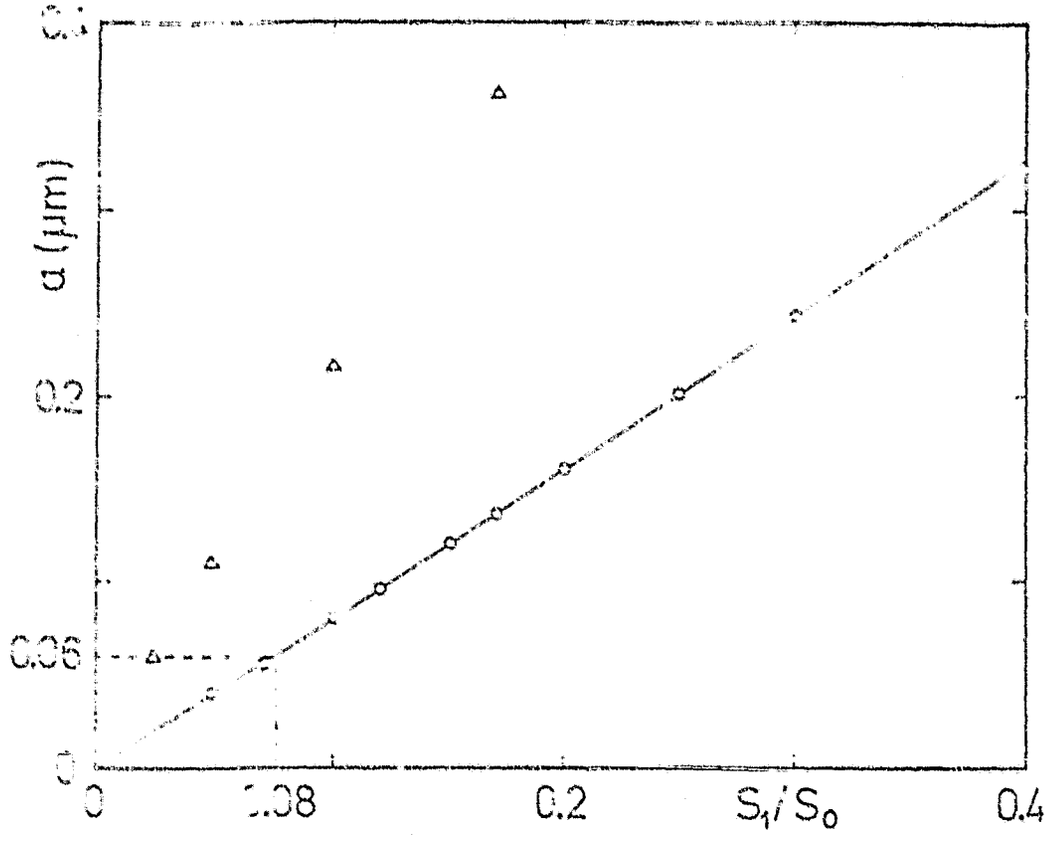

Figure 6: Amplitude of the support point error as a function of the behavior of the intensity of a secondary line S_1 and the intensity S_0 of the primary line. Plotted curve: analytically determined relation for the zero points of a secondary line (equation 3.8). Points: numerically determined error amplitude of the zero transits.

○ for a secondary line
△ for three secondary lines of the same intensity

measurement (wave number $\tilde{\nu}_F$), from equations 2.3 and 3.8 we obtain the following equation for small intensity ratios S_1/S_0:

$$3 - \frac{S_1}{S_0} \qquad (3.9)$$

/18

The pair of ghost lines accompanying each spectral line may not exceed a relative peak of 10^{-2} in the GIRL interferometer in order not to deteriorate the quality of the spectrum. For the case of a secondary line from equation 3.9 we obtain the maximum permissible intensity by substituting $\tilde{\nu}_F$ = 500/cm and $\tilde{\nu}_1$ = 2000/cm as 8% of the primary line intensity. By superimposition of the support point error upon the occurrence of several secondary lines, an approximately linear relationship exists between the intensity of the ghost lines in the Fourier spectrum and the total intensity of the secondary lines

in the laser spectrum. Thus, as an upper limit of total intensity we also have a fraction of 8%. This requirement consequently follows from the permissible maximum value of the support point error of 0.06 μm, which results from the limitation of the ghost line peak (equation 2.3). The support point error occurring here is proportional to the laser wavelength (equation 3.9). Therefore, the intensities of the ghost lines can be reduced by shortening $\tilde{\nu}_L$ whereby less rigid requirements result for the level of the secondary lines.

With regard to the limitations of signal amplitudes caused by position electronic system (1.9 V $S_0 \leq 5$V), the periodic fluctuation in the interferogram amplitude is important (Figure 5). A secondary line with the maximum permissible intensity (8%)leads to an amplitude fluctuation of between 85% and 100% of the maximum amplitude S_0+S_1, the same is true for several secondary lines. Thus, for optical alignment of the signal to the input of the position electronic system, the amplitude values thus lie between 5V and 4.2V. Under consideration of the reduction caused by line width, the minimum amplitude is about 3.8V, which clearly lies above the lower limit of 1.9V. The required intensity relationships in the laser spectrum consequently do not result in additional reduction in support point accuracy as a result of the behavior of the signal amplitude, so that the named requirements for the existance of a useful laser interferogram are guaranteed.

3.1.2 Constancy of Wavelengths /19

In the determination of the separation of the ideal support points, the wavelengths of the reference beam are important. Fluctuations in the wavelengths during recording of the main interferogram invalidate the feed monitoring system. For diode lasers, changes in wavelength come into being primarily through fluctuations in the bath temperature. With changing wavelengths λ_L, the optical path difference differs from the ideal value x_n for the same number of transitive support points (n). If we consider the slow drift in wavelength λ_L proportional with time, then this can be described as a function of the optical path difference x for constant feed velocity:

$$\lambda_L = \lambda_0 \cdot c \cdot x \qquad (3.10)$$

(c = const.). From the positions of the new support points x_n':

$$x_n' = \frac{n \cdot \lambda_L(x_n')}{4} \qquad (3.11)$$

there follows, by application of equation 3.10, the changed maximum optic path difference L' with n = total number of support points N (N = 320000, see Section 2.2) as:

$$L' = \frac{1}{1 - \frac{Nc}{4}} \cdot \qquad (3.12)$$

With the requirement that these actual transited path differences differ from the ideal value L only by one-tenth of the support point

separation ($\lambda_0/40$): [illegible] .125 µm

there results the maximum permissible shift in wavelength:

[illegible] . (3.13)

With the named values, the requirement of wavelength fluctuation during observation is thus [illegible] For a line shift of a diode laser by 0.2/cm/degree (see Section 4.1.3), a stabilization of the bath temperature at $3 \cdot 10^{-3}$ K is thus necessary.

3.2 Requirements of the IR Detector /20

The important parameters of a IR detector are spectral sensitivity range, detectivity and time constance. The sensitivity range is adjusted here to the wavelength of the reference radiation (ca. 5 µm). The requirements of time constance (speed) of the used detectors are determined by the permissible phase shift between incident radiation signal and detector output signal. The requirements of detectivity are specified by the S/N ratio which is needed to determine the readout points. These relationships are discussed below.

3.2.1 Detectivity

In section 2.2 we were able to determine that to achieve a readout accuracy of $\Delta x = v\tau$ (or $2v\tau$) at the support points, the S/N ratio must be ≥ 800 (see Section 4.4). The size of interferometer signal is determined by the power output P in the reference beam, the optical properties of the beam splitter and the other optical components as well as by the response capability R (responsivity) of the detector. The responsivity is defined as the quotient of the electrical signal S at the detector output and the incident radiation signal P which generates the output signal:

$$R = \frac{S}{P}$$

Under the assumption of complete reflection at the mirrors of the interferometer and a loss-free imaging of the interferometer beam on the detector, for the amplitude S_0 of the interferometer signal ($S_0 = S/2$) we have:

$$S_0 = 2r_0 t_0 \cdot R \cdot P \ . \qquad (3.14)$$

The factors R_0 and t_0 denote reflection and transmission of the beam splitter, the so-called effectiveness $4r_0t_0$ is generally ≤ 0.8 for the beam splitter foils used. This signal contains noise components generated by the photon noise of the background radiation and by internal detector effects (Hudson, Hudson 1975). If the total observed noise voltage is N at a measured bandwidth Δf, then the noise voltage standarized to a 1 Hz bandwidth is calculated as: /21

[illegible] . (3.15)

The [illegible]uivalent power (NEP) is defined as that incident radiation p[illegible] which generates an output signal equal to the effective value of the detector noise voltage n at a given responsivity and measured bandwidth of 1 Hz:

(3.16)

For a given signal to noise ratio S_o/N and predetermined radiation power P we can calculate the NEP needed for the experiment from equations 3.14 to 3.16.

[illegible] (3.17)

According to the definition, the detectivity D is the inverse value of the NEP. (The most often given characteristic quantity D* is the quantity D standarized to the unit surface of the detector element.) For an anticipated emission power in the reference beam of 10 μW and a beam splitter efficiency of 0.8, a S/N ratio of 800 can be achieved for an amplitification bandwidth of 10,000 Hz by a detector whose NEP is $5 \cdot 10^{-11}$ [illegible] maximum. Signal losses and non-optimum tuning of beam splitter efficiency require a approximate 5 to 10 fold greater minimum detectivity in practical cases. Thus, for the interferometer a high sensitivity detector is needed whose output signal is tuned by an amplifier to the amplitude requirements of the input of the position electronic system. The contribution of the amplifier to the total noise voltage must not notably reduce the required input S/N ratio of ≥ 800.

3.2.2 Time Constance /22

The time constance of the detector significantly determines how accurately the voltage profile at the output will reproduce the actual intensity profile at the detector element . This quantity is called the response time. It is the time difference between the switch-off time of an incident radiation signal and the drop in voltage signal S to $S \cdot \exp(-1)$. The response time of the positioning electronic system (integration time) is $\tau_p = \frac{1}{12\sigma}$. For the known values [illegible] we obtain $\tau_p = 10^{-4}$s. As a chronological resolution of the curve at the detector, a value smaller by a factor of 10 than the resolution time of the position electronic system is desireable. The desired response time of the detector τ_D is thus 10 [illegible]sec and causes a constant shift between beam and voltage signal of $\Delta x = v \cdot \tau_{..} = 0.004$ [illegible]. This constant phase shift of the curve or of the readout points causes a change in the transformed spectrum. The curve profile should be resolved by the detector with this accuracy so that the support point errors are caused only by the position electronic system. IR detectors with response times of less than 10 [illegible]sec are therefore suitable for the feed monitoring system.

3.3 Requirements of the Beam Splitter /23

For the Michelson interferometer presently under construction,

thin mylar foils (PET foil) are provided for use as beam splitters. Because of their low absorption losses in the far infrared, they are quite suitable and furthermore, they can be used even with the laser reference wavelength. Very little information is available about their low temperature behavior. The relations summarized below will permit optimization of the beam splitter.

The beam splitter of the Michelson interferometer splits the incident beam bundle (amplitude A_i) into a reflected (amplitude A_r) and a transmitted (amplitude A_t) bundle. If we neglect the absorption, at the detector (after a transmission and reflection) we obtain a bundle of amplitude E for constructed interference:

$$E = 2 \cdot \frac{A_r A_t}{A_i}$$

The effectiveness of the beam splitter is defined as the fraction of incident intensity which reaches the detector, thus we obtain the following equation with $r_o = (A_r/A_i)^2$ and $t_o = (A_t/A_i)^2$:

$$e = \frac{E^2}{A_i^2} = 4\, r_o t_o \cdot \qquad (3.18)$$

The maximum value e = 1 is obtained for $r_o = t_o = 0.5$. With dielectric beam splitter foils, numerous parallel transmitted and reflected wave trains originate through multiple partial reflection of the beam spreading out in the foils; these wave trains interfere with each other (Figure 7). Below, we derive r_o and t_o as a function of phase difference of neighboring beams and under consideration of absorption in the medium. The reflection coefficients r_p and r_s for a reflection of parallel or perpendicular polarized radiation at a surface of the dielectric satisfy the Fresnel equations (Born, Wolf 1959):

$$r_p = \frac{\tan^2(\theta - \theta_1)}{\tan^2(\theta + \theta_1)} \quad ; \quad r_s = \frac{\sin^2(\theta - \theta_1)}{\sin^2(\theta + \theta_1)}$$

where the angle of incidence is designated as θ, the refractive angle as θ_1. The corresponding transmission coefficients t_p and t_s supplement r_p or r_s to form one. For unpolarized radiation the reflection coefficient r and transmission coefficient t are: /24

$$r = \frac{1}{2}(r_p + r_s) \quad ; \quad t = \frac{1}{2}(t_p + t_s) = 1 - r$$

The phase difference of neighboring beams is (see Figure 7):

$$\delta = 4\pi \bar{\nu} n \cdot d \cdot \cos\theta_1 \cdot \qquad (3.19)$$

By absorption in the beam splitter the intensity of the beam is reduced for one transit of the foil by the fraction "a" of the initial intensity.

$$a = \exp\left(-\frac{\alpha \cdot d}{\cos\theta_1}\right)$$

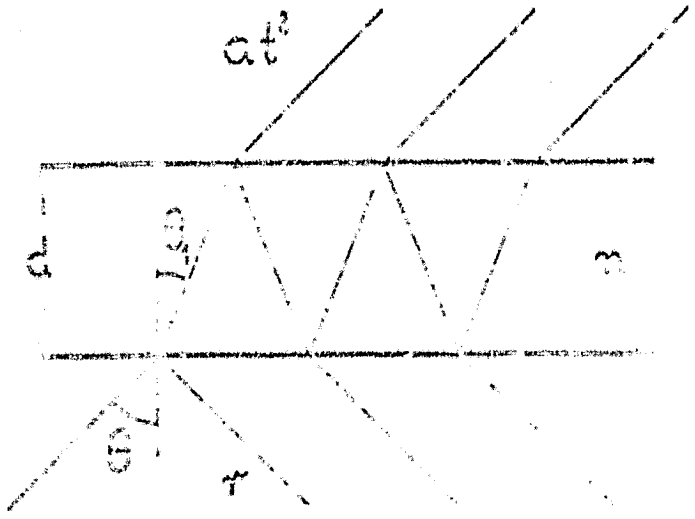

Figure 7: Illustration of the split of an incident beam (incident angle θ) at the surface of the beam splitter (refractive index n, refractive angle θ_1, thickness d). R: fraction of the power reflected at a surface. at^2: fraction of transmitted power for double surface transmission and absorption losses.

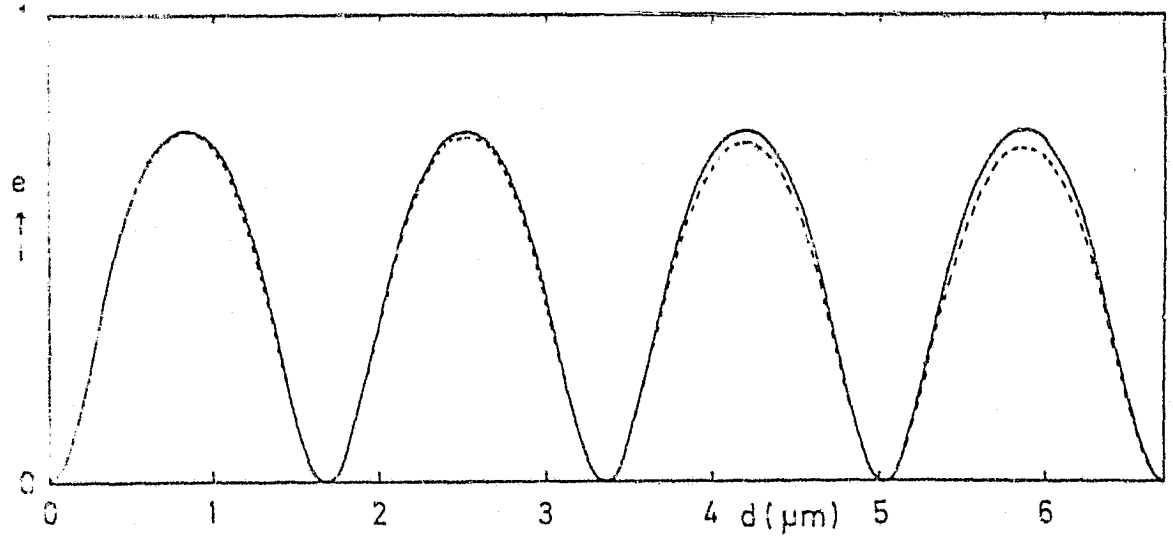

Figure 8: Dependence of effectiveness on foil thickness while keeping the wavelength constant (λ = 5 μm) with and without absorption (typical absorption coefficient $\varkappa$ = 0.005/μm)

Here, α is the length absorption coefficient.

By summation over the interfering beams the coefficients of the total reflection r_o and total transmission t_o can be obtained (Naylor et al. 1977).

$$r_o = \frac{\quad}{\quad} \; ; \; t_o = \frac{\quad}{\quad} \qquad (3.20)$$

Thus, from equation 3.18 we obtain the following expression of the efficiency of the beam splitter: /25

$$e = \frac{\quad}{\quad},$$

for negligible absorption (a = 1)

$$e = \frac{\quad}{\quad}. \qquad (3.21)$$

By means of the given formulas the characteristics of the beam splitter are now determined. The material constants of mylar are now:

Refractive index: $n \approx$ 1.6[illegible] at $\lambda \approx$ [illegible] μm (Du Pont)
$n \approx$ 1.7[illegible] for $\lambda >$ 20 μm
(Smith, Loewenstein 1975)

Absorption coefficient: $\alpha \approx$ 0.005/μm at $\lambda = 5\ \mu$m
(Du Pont)

For specified wavelengths Figure 8 shows the influence of absorption: the efficiency drops increasingly with increasing foil thickness compared to the values without absorption, the periodicity of the curve profile e(d) is retained however.

The decisive modulation of the efficiency comes into being through the term cos δ (periodicity). The wavelengths for radiation on optimum foil densities (maximum efficiency) are obtained from cos $\delta = -1$ as (see Equation 3.19): /26

$$d = \frac{2k+1}{4 \cdot n \cdot \cos\beta} \cdot \lambda \qquad k = 0, 1, 2, \ldots \qquad (3.22)$$

The best spectral ranges for mylar foils of various thickness can be seen in Figure 9. For the GIRL Michelson interferometer several foils with different windows in the far infrared range can be used. For instance, a mylar beam splitter 6 μm thick is suitable for a reference wavelength of 5 μm and an astronomic useful spectral range of about 25 - 75 μm.

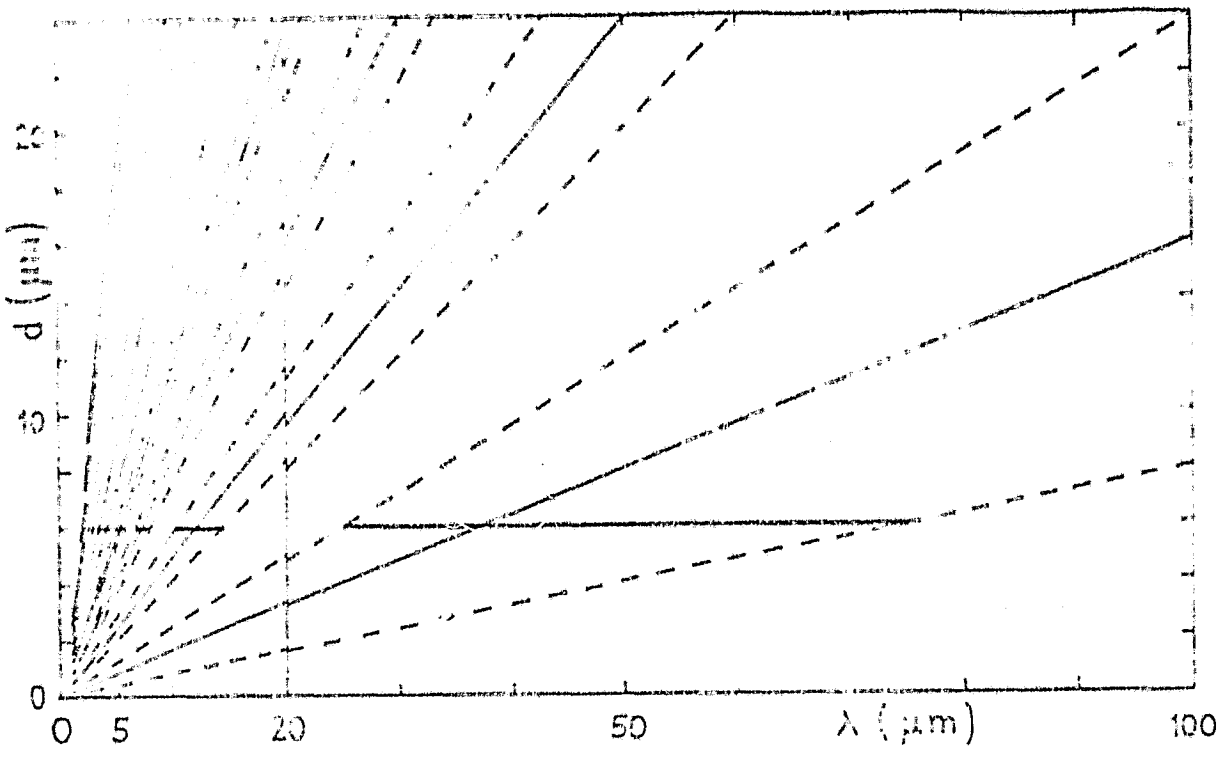

Figure 9: Relation between foil thickness and wavelength for maximum effectiveness e_{max} (solid lines) and at 0.66 e_{max} (dashed lines). Values of refractive index used: $\lambda < 20$ μm: n = 1.65, $\lambda > 20$ μm: n = 1.71. The horizontal bars illustrate the best spectral range of a foil of 6 μm thickness. The effectiveness is not constant on the straight lines since the absorption increases with increasing thickness and also depends on the wavelength.

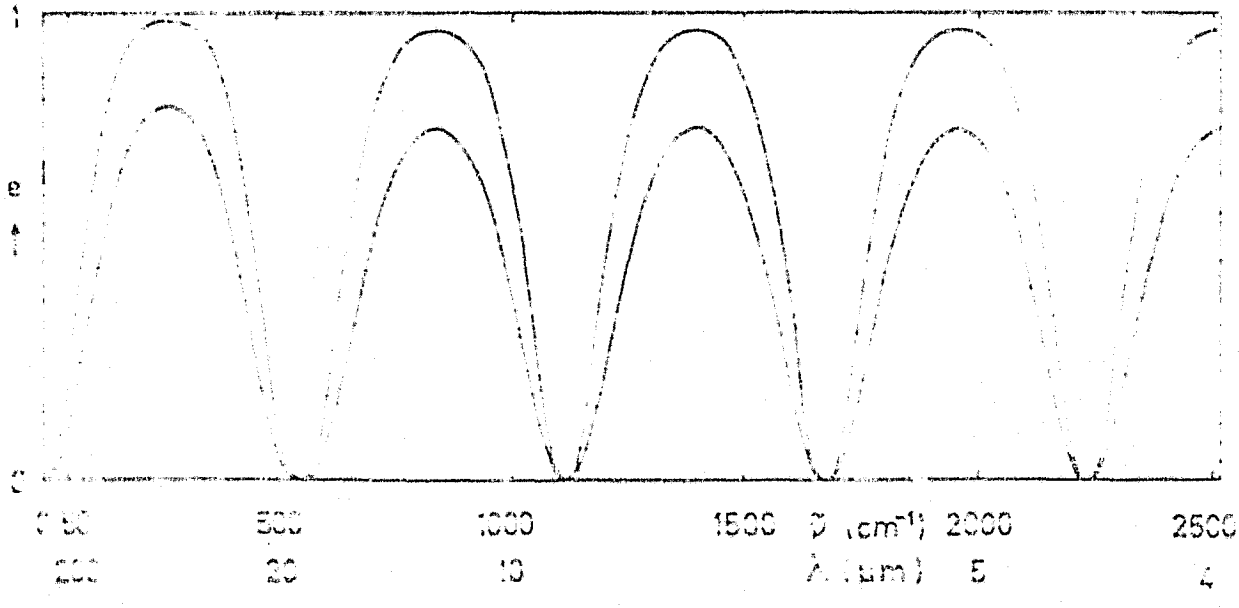

Figure 10: Relation between the effectiveness and wavelength using the example of the 6 μm-foil without regard to absorption. Upper curve: light polarized perpendicular to the incident plane; lower curve: non-polarized light.

For a foil d = 6 μm thick, the beam splitter efficiency according to equation 3.31 for variously polarized light is calculated and illustrated in Figure 10 by neglecting absorption. For radiation polarized perpendicular to the incident plane, the efficiency values are maximum; at the maximum of the curve the ideal value e = 1 is approximately reached. As a result of absorption by the foil, the true efficency values are smaller than the calculated values. The average absorption in the important spectral ranges only result in minor effects whose approximate size can be read off from Figure 8 at d = 6 μm. /27

4. Experimental Studies on the Main Components of the Feed Monitoring System

4.1 The Semiconductor Diode Laser

4.1.1 Principle of the Diode Laser

A semiconductor diode laser is a radiation emitting semiconductor diode which is a Fabry-Perot-Resonator (Figure 11). Pumping the laser takes place through injection of electrons and deficit electrons in the recombination region at the p-n-transition. Through application of an external voltage in the transit direction of the diode, electrons and deficit electrons are injected into the conductance band or valence band of this active zone (Figure 12), where they recombine under the emission of a light quantum (photon). The resonator axis runs parallel to the space charging zone since the absorption losses are smallest there. Diode lasers posess a continuum of population inverted states which leads to simultaneous amplification of several resonator modes. In general, the laser therefore emits a line spectrum; the line widths are determined by effects of spontaneous emission and environmental influences. The population of high energy levels upon increasing the supply voltage leads to a shift in intensity to resonator modes of shorter wavelength (mode hopping), the temperature increase through the Joule peak connected with diode current causes a change in the refractive index and thus a spectral shift of modes (continuously tunable). Constant laser temperatures and currents are therefore the prerequisites for constant emission characteristics. In diode lasers, besides the axis parallel modes, standing waves are also amplified with non-axis parallel propagation direction. Therefore, the emission of several beam bundles is normal, whose divergence is determined by diffraction effects upon exit from the very small emitting surface. This results in large openings of the laser beam bundle (typical opening angle 30 degrees). The power output of the different diode lasers lies roughly in the range between microwatt and milliwatt and can be varied along this range by the diode current. Detailed discussions of semiconductor lasers and of the other semiconductors are found for instance in Nathan 1966, Rieck 1968 or Kressel 1971. /29

Measurements were performed on three laser diodes. Among them were two lead salt diodes (AEG-Telefunken, Frankfurt, Company, Material $PbS_{1-x}Se_x$ x=0.4, Nr. DH 399 8/1-A; Laser Analytics, Company Inc., Bedford, USA, Mod. SDL 20, Nr. 8362-1), whose specifications given by the manufacturer indicated their use as reference emission sources. We are dealing with laser diodes with a wavelength near 5 μm which

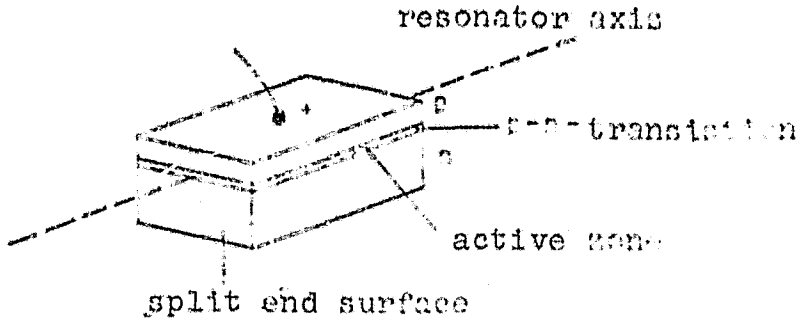

Figure 11: Schematic illustration of the laser diode. The resonator axis lies in the p-n-transistion, the resonator cavity is bounded by two crystal surfaces formed by splitting at parallel grid planes.

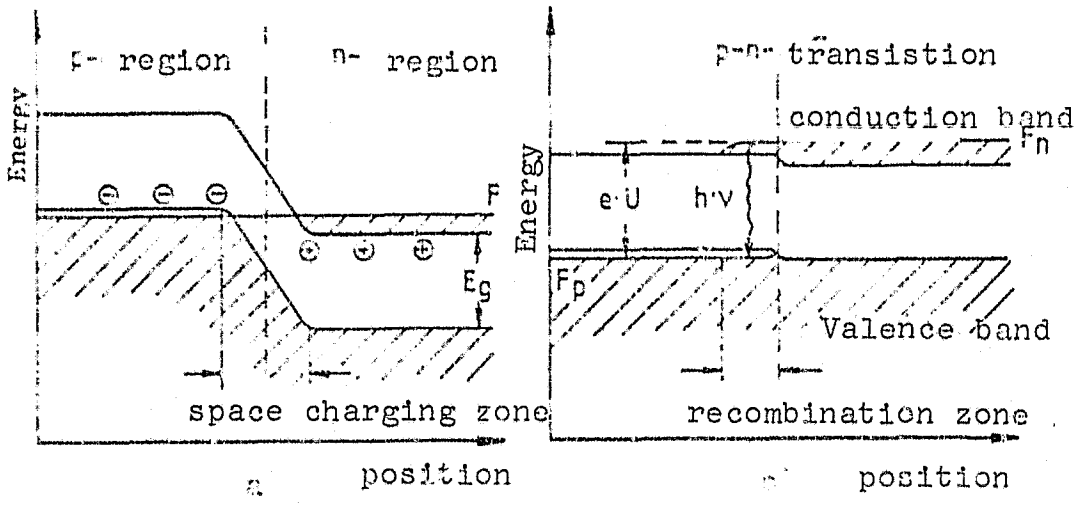

Figure 12: Band model sketch of a laser diode (a) without external potential, (b) with applied supply voltage U. E_g: band edge separation between conduction and valence band. F_n, F_p: quasi-fermi potentials of the n- and p-zone. Populated levels are shown by slash marks.

can only be operated at temperatures below 30K. In addition, a GaAlAs-Diode was studied; it emits at a wavelength of about 1 μm (AEG-Telefunken, Ulm, Nr. UV 18 P1 ZJ E 3). It is normally designed for operation at room temperature but can also be used at low temperatures. All studies were performed in a vapor cryostat at a temperature of boiling nitrogen (77 K) or helium (4 K).

In the following sections the laser measurements are described; /30
these are needed to determine their utility as reference emission source in the feed monitoring system. The operation of diodes takes place with a direct current unit designed specifically for this (Laser control unit, Fa. Arthur D. Little, Cambridge, USA). The diode current is kept constant by this unit to an accuracy of 10^{-4} A, whereby a current stabilized laser operation is guaranteed.

4.1.2 Study of the Spectral Intensity Distribution

The spectral intensity distribution was decisive for the use of the diode laser in the feed monitoring system. The corresponding requirement has been derived in Section 3.1.1. By recording of spectra the laser emission is studied. The objective of the measurements was to find a working point (diode current) of the laser diode so that the total intensity of the secondary lines amounts to no more than 8% of the intensity of the main line. To study the spectral intensity distribution, a Monochromator (Mod. 218, McPherson Instrument Corp., Acton, USA) was used. This instrument achieves a spectral resolution of 0.8/cm at a wavelength of 1 μm with appropriate grid (1200 lines/mm); at 5 μm with appropriate grid (75 lines/mm), the resolution is 0.4/cm. Therefore, with this unit we cannot check whether the line widths of the laser are less than $3 \cdot 10^{-4}$/cm and consequently, the modulation of the interferogram is influenced only to the minor extent desired (see Section 3.1.1, Equation 3.2). The test setup of this experiment is shown by Figure 13; the schematic setup with beam path is seen in Figure 14. As a result of the inlet crevice of the monochromator and after splitting into several orders (5 for visible light), only an extremely small fraction of the beam power of the divergent bundle reaches the outlet crevice. These intensities are too weak to generate a useful S/N ratio with existing IR detectors (see Chapter 4.2). Therefore it is necessary to focus the beam bundle onto the inlet crevice, whereby the divergence of the bundle in the monochromator must be kept small. Antireflection coated Germanium lens are used for this. Thus, the power output at the detector can be increased over the system without collimation by about two orders of magnitude. Through the use of a lock-in amplifier (Mod. /31
Dynatrac 3, Fa. Ithaco, Ithaca, USA), it is possible to record useful spectra at laser power outputs of a few μW, in spite of the still considerable interference noise. Behind the outlet crevice, the radiation is recorded by the Golay detector (model IR50, Cathodeon Company) or by a photovotaic InSb detector made by Barnes Company. A short description of these detectors is found in Section 4.2. The voltage signal delivered by the detector comes into being through the periodic alternation between laser emission and inherent emission of the chopper--whereas the laser beam is covered. This alternating /32
current signal is amplified by a preamp which is adapted to the

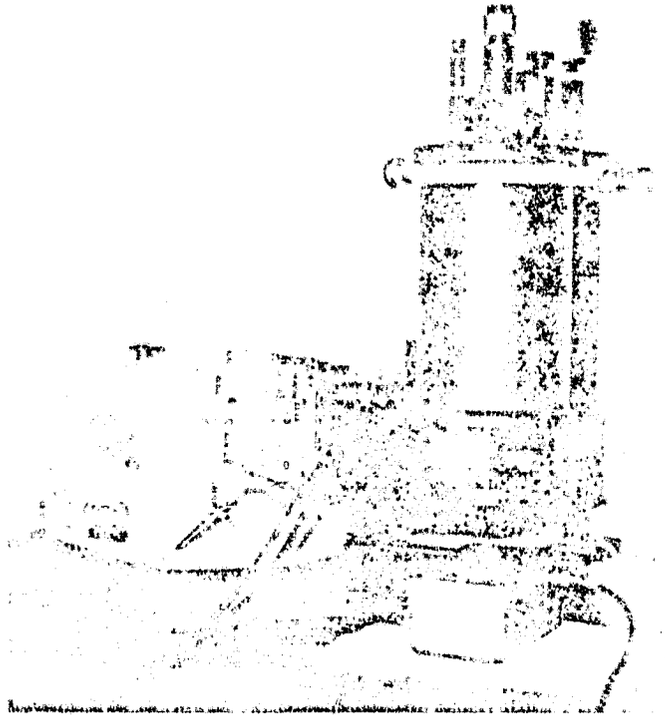

Figure 13: Test setup for spectral study of the laser beam

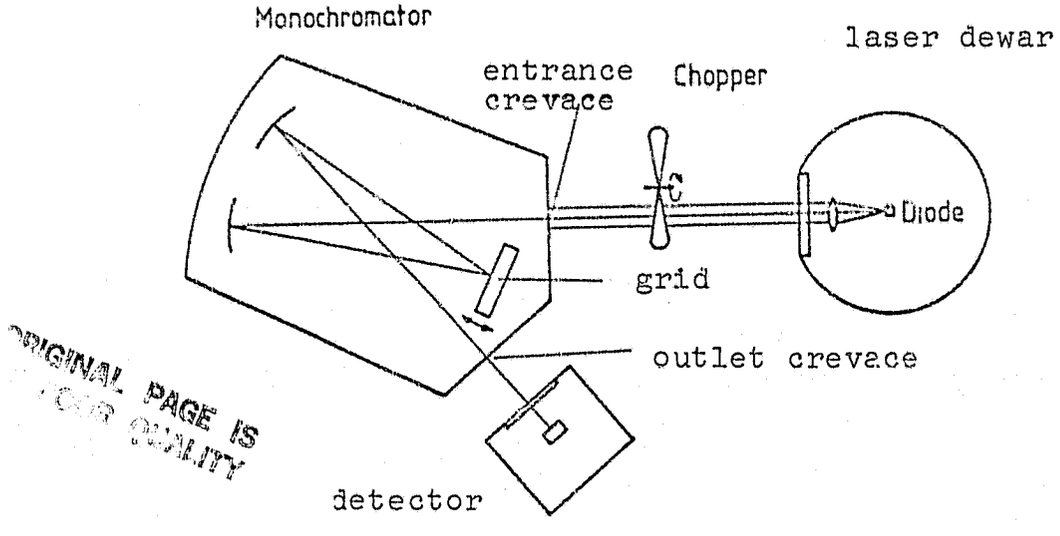

Figure 14: Sketch of the test setup with beam path.

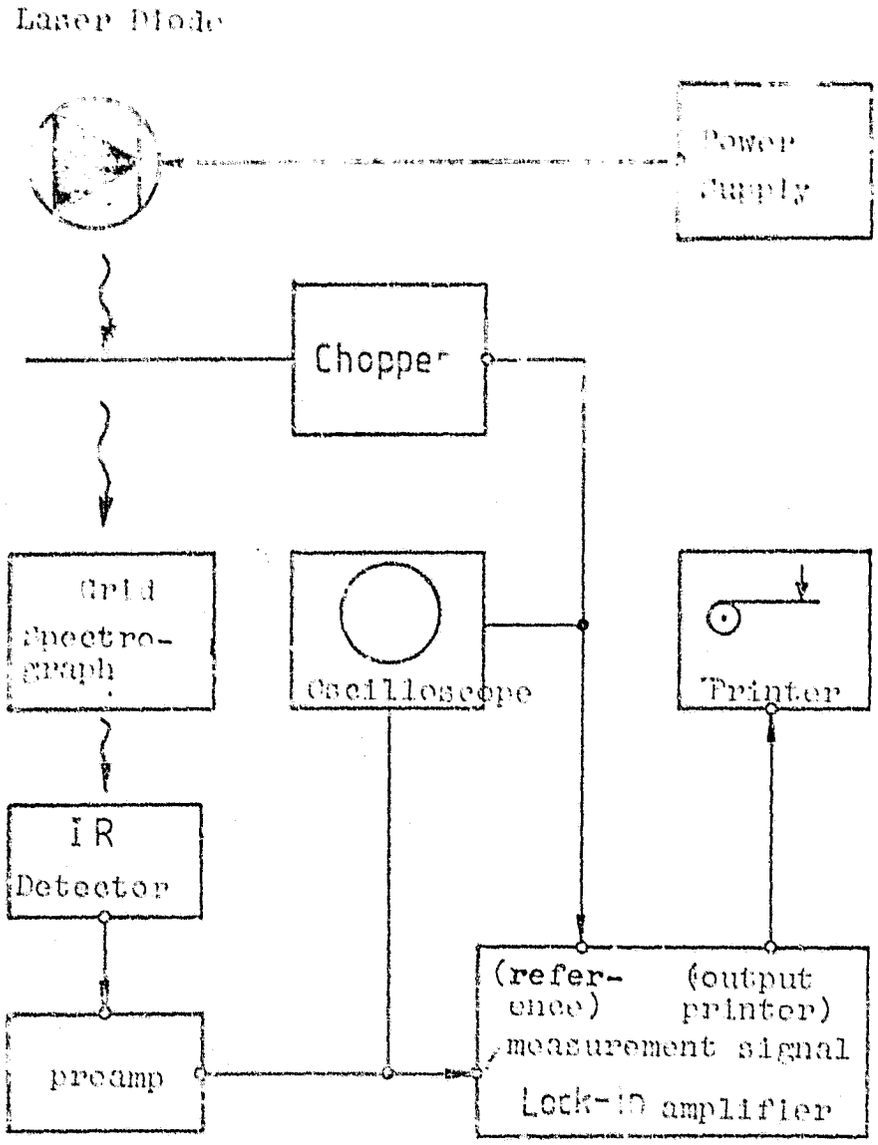

Figure 15: Block diagram to record the laser spectra

particular detector, and by the lock-in analyzer. The d.c. signal at the output of the lock-in amplifier is recorded by a printer. Figure 15 shows the block diagram of the test. Numerous laser spectra were taken; the change in spectral characteristics was tracked after systematic variation of the diode current. The important properties of the spectra for different diode currents (among them also the working point) are summarized in the table given below.

The corresponding spectra are shown in Figures 16, 17 and 18. The typical mode separation of the lead salt diodes is 2/cm. A suitable working point could only be found for the lead salt diodes. However, the spectral of the Gallium diode always exhibits several modes. This laser--suitable for use at room temperature--could also

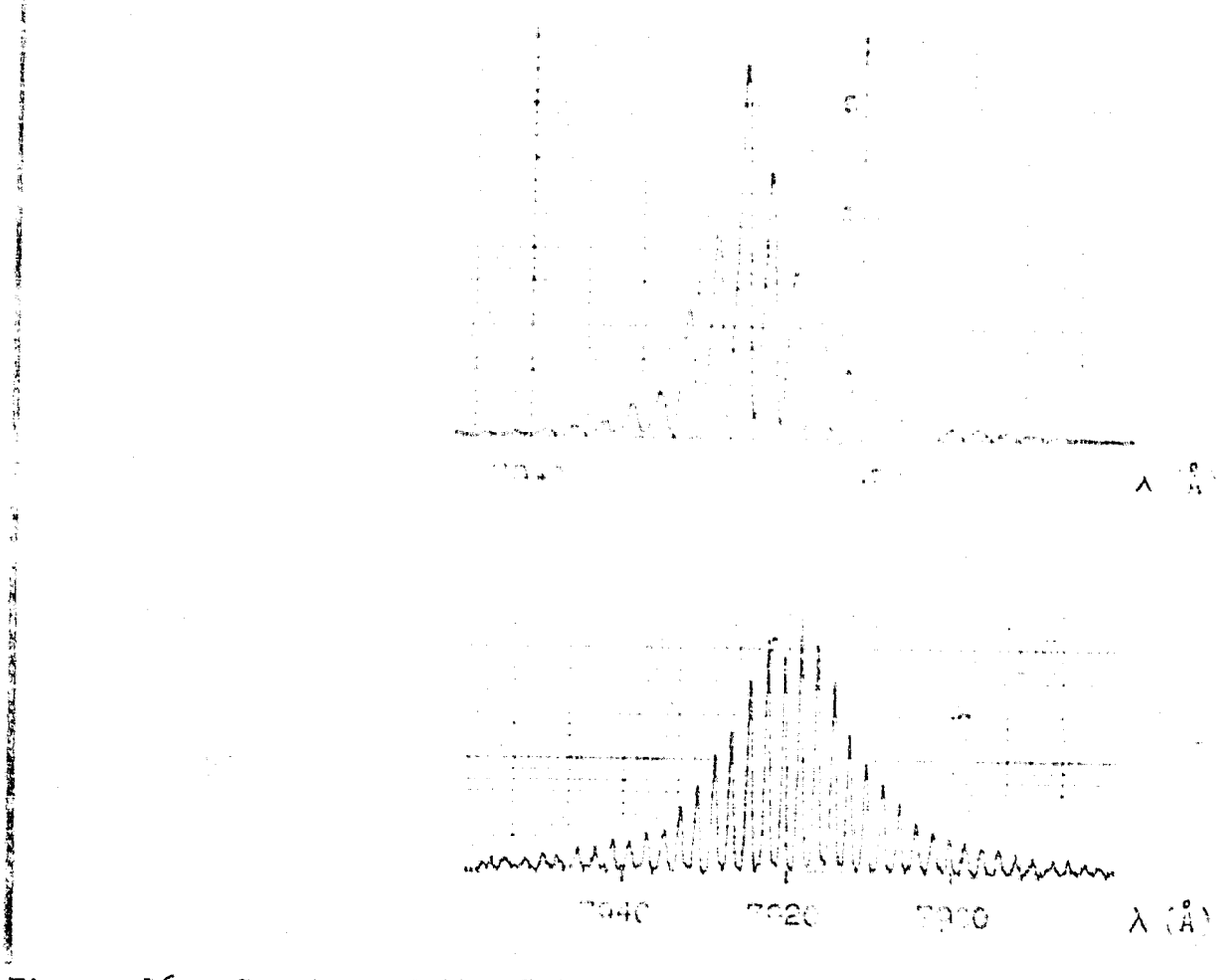

Figure 16: Spectra of the CaAlAs-Laser at 77 K and a diode current of 80 mA (a) or 150 mA (b)

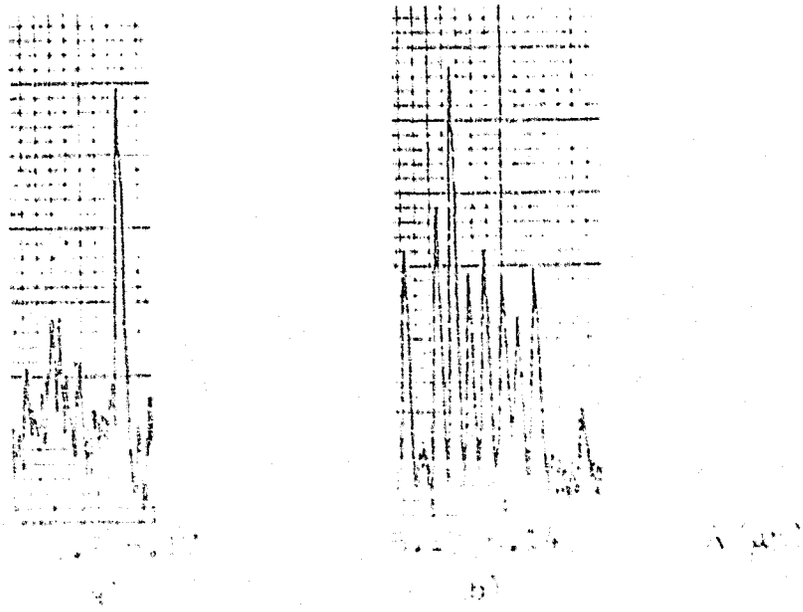

Figure 17: Spectra of the 5.2- μm-lead salt laser at 4 K at the working point (920 mA) (a) and at 1.3 A (b)

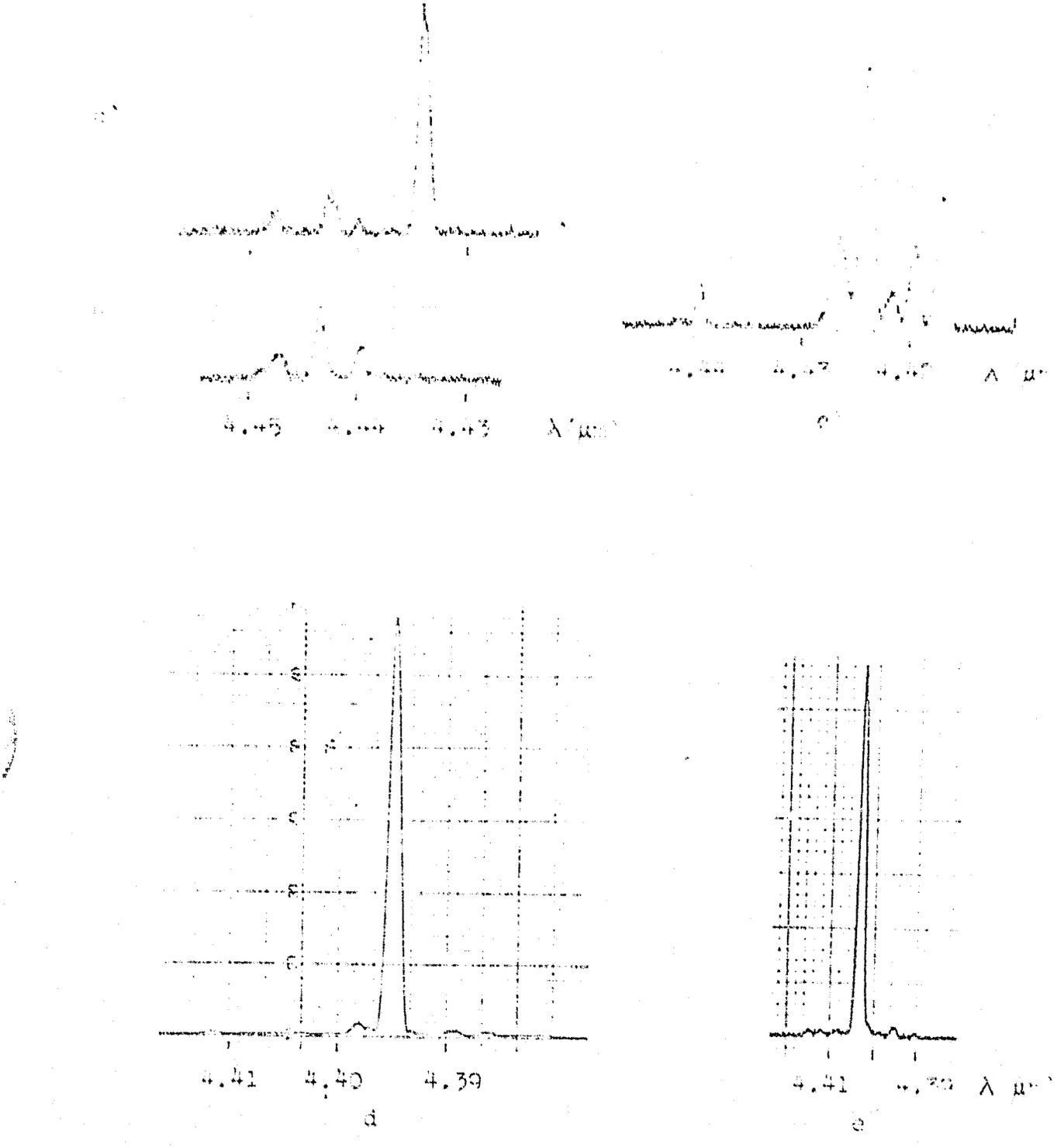

Figure 18: Spectra of the 4.4- μm-salt laser at 4 K and diode currents of 144 mA (a,b), 600 mA (c), 1.132 A - working point (d) 0.959 A - later working point (e)

Working Temperature	Diode Current	No. of lines	Intensity fraction of secondary lines	Wavelength at working point (μm)
				5.184 ± 0.001
				4.3956 ± 0.0005
				4.4036 ± 0.0005
	New working point after changing test setup near diode			

be operated at 77 K. Attempts to test the laser at a bath temperature of 4 K (GIRL conditions) failed. With decreasing operating temperature, the Ohm resistance of the diode increased quickly (to more than 20 k Ω), so that at helium temperature, the threshhold for laser activity could not be exceeded with the permissible bias. The spectra have several modes of comparable intensity with a typical, schmetric envelope (Figure 16). With increasing diode current the number of excited modes increases. For these reasons, the laser is unsuitable for the intended feed monitoring system. A useful ratio of line intensities of main and secondary lines is found for the two 5 m diodes. The working point of the 5.2 μm laser lies near the threshhold for laser activity at ca. 0.9 A, for higher currents other modes can be added (Figure 17). These spectra posess an irregular structure. The working point of the 4.4 μm diode lies in the middle of the range of laser activity, namely, between 1.128 A and 1.135 A, at higher and lower currents spectra with stronger secondary lines are obtained. Near the threshhold for laser activity (diode current ca. 90 mA) the spectra cannot be reproduced after intermediate heating of the laser to room temperature and subsequent recooling (Figure 18a, b). Necessary changes in the test setup resulted in a shift in the working point to 0.959 A (Figure 18e). The working points of the diodes were also slightly affected by the temperature cycles. These effects are stressed in the following section. /36

4.1.3 Study of the Stability of the Working Point

Regarding this subject, sufficient data are only available for the 4.4 μm laser, since the 5.2 μm diode could no longer be operated before conclusion of the measurements. As a result of the frequent cooling and heating processes (temperature cycles), a contact at the crystal loosened and it could no longer be repaired by the manufacturer.

With repeated recording of the spectra of the 4.4 μm diode, the working point was tracked during operation and over several temperature cycles (Figure 19). The measurement points were taken after cooling in liquid helium; between the measurements the laser was brought to room temperature. With the exception of the shifts due to changes in test setup near the diode (influencing the heat contact), the working point behaves generally stationary. The shifts in the diode current after a temperature cycle are less than 10 mA, that of the wavelength is less than 2 nm. While the diode was at operating temperature, maintained by the cold bath, no changes were measured. Fluctuations in wavelength could thus be estimated at maximum 5 Å. The favorable boundary conditions on GIRL permit a stable operation of the laser, so that maintenance of required wavelength consistancy (Section 3.1.2) can be expected. After implementation of the changes, the working point had to be redetermined.

/37

Figure 19: Diode current I and wavelength λ_L at the working point over several temperature cycles.

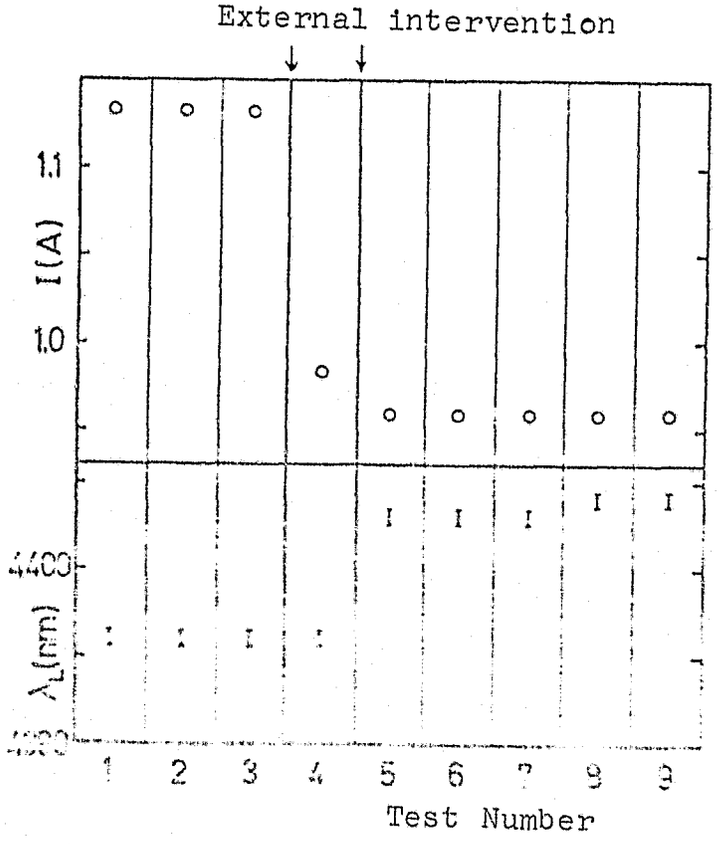

4.1.4 Measurement of Spatial Intensity Distribution

Diode lasers, in contrast to standard lasers, posess a divergent beam bundle which comes into being through transversal modes (Paoli et al. 1969) and by diffraction expansion at the very small emitting surfaces. In the position interferometer, a parallel laser beam bundle is needed as a reference; its diameter is limited to about 3 mm, thus the cross-section of the main beam bundle cannot be reduced very much. For collimation of the beam bundle, an optic lens is needed and the opening angle of the beam cone of rays must be determined in order to design this lens. For this purpose, an isophoton map of the intensities was prepared in the divergent bundle by means of a raster scanning method. As detector, we used a Golay cell with preset perforated apperture (diameter: 2 mm). As a separation for the raster points, 2 mm was selected. At a distance of the apperture from the laser of between 7 and 11 cm--corresponding to an angular resolution of 1.0 degrees to 1.6 degrees--the majority of the bundle was detected at the maximum extent of the raster of 30 mm. Only the intensity attenuation at edge zones is ignored in this measurement. Under the given geometric conditions, projection effects due to oblique incidence onto the perforated apperture can be neglected. To separate the laser from the background signal, the laser beam is internally modulated by feed of a rectangular current. Thus, the diode temperature is subject to fluctuations so that minor deviations of radiation characteristics compared to stable current operation are found. Figure 20 shows the chronological intensity profile of the laser radiation at the working point. At a modulation frequency of 13 Hz, definite deviations from the constant intensity profile upon switch-on of the current are seen. It was also attempted to modulate the radiation by means of a chopper wheel, however its inherent emission was too intense to permit the measurement. The detector signal is measured by a lock-in amplifier whereby the modulated supply voltage serves as a reference signal. The block diagram of the test is shown in Figure 21. The isophoton maps are illustrated in Figure 22. The beam bundles near the threshhold for laser activity exhibit an intensity distribution declining constantly outward (Figure 22b, c). At greater currents, the 4.4 μm laser has a definite transversal mode structure (Figure 22a). The characterization of the divergents required determination of the whole opening angle at half maximum intensity. It is 15° at the working point (1.132A) of the 4.4-μm diode; at lower currents (120 mA), it is likewise 15°, because of the general insensitivity to operating conditions, this opening angle can also be anticipated for continuous operation of the laser, likewise at the new working point (0.959 A), which resulted from the changes in the test setup needed to collimate the bundle, whereafter the spatial intensity distribution could no longer be measured. The fraction of power output in the cone of opening angle of 15° was estimated at 50% of the total power output. Collimation of the divergent bundle with a suitable optic lens is described in Section 5.1.

/38

/39

4.1.5 Measurement of the Emission Power Output

/42

The emission power output of the laser diode at the working point

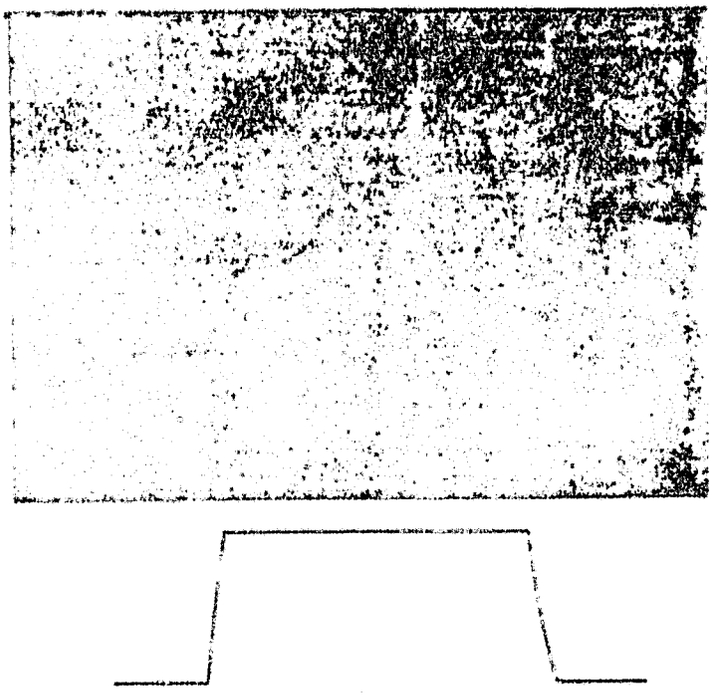

Figure 20: Laser signal plotted against time (top) for rectangular modulated diode current (bottom)

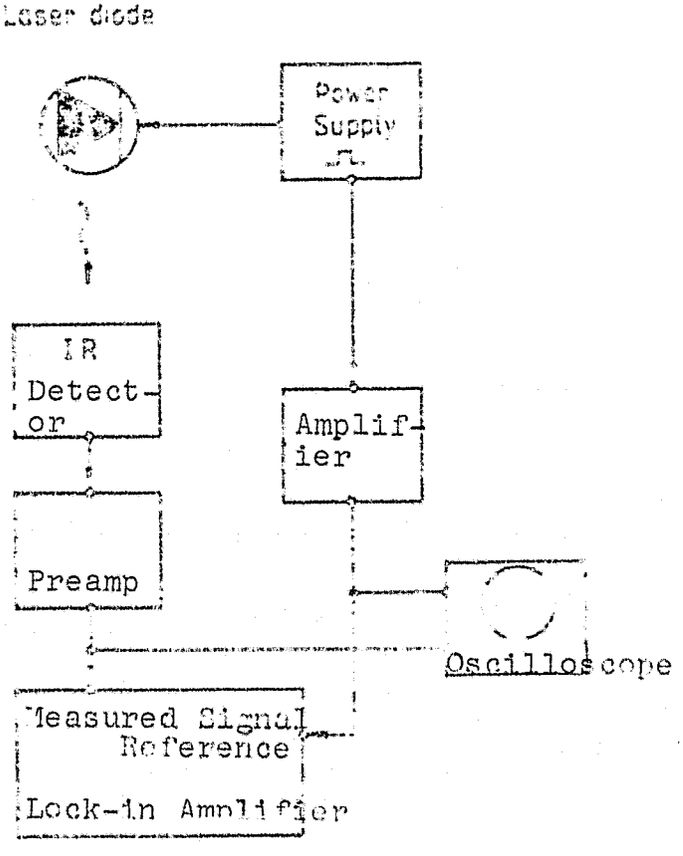

Figure 21: Block diagram to measure the spatial intensity distribution

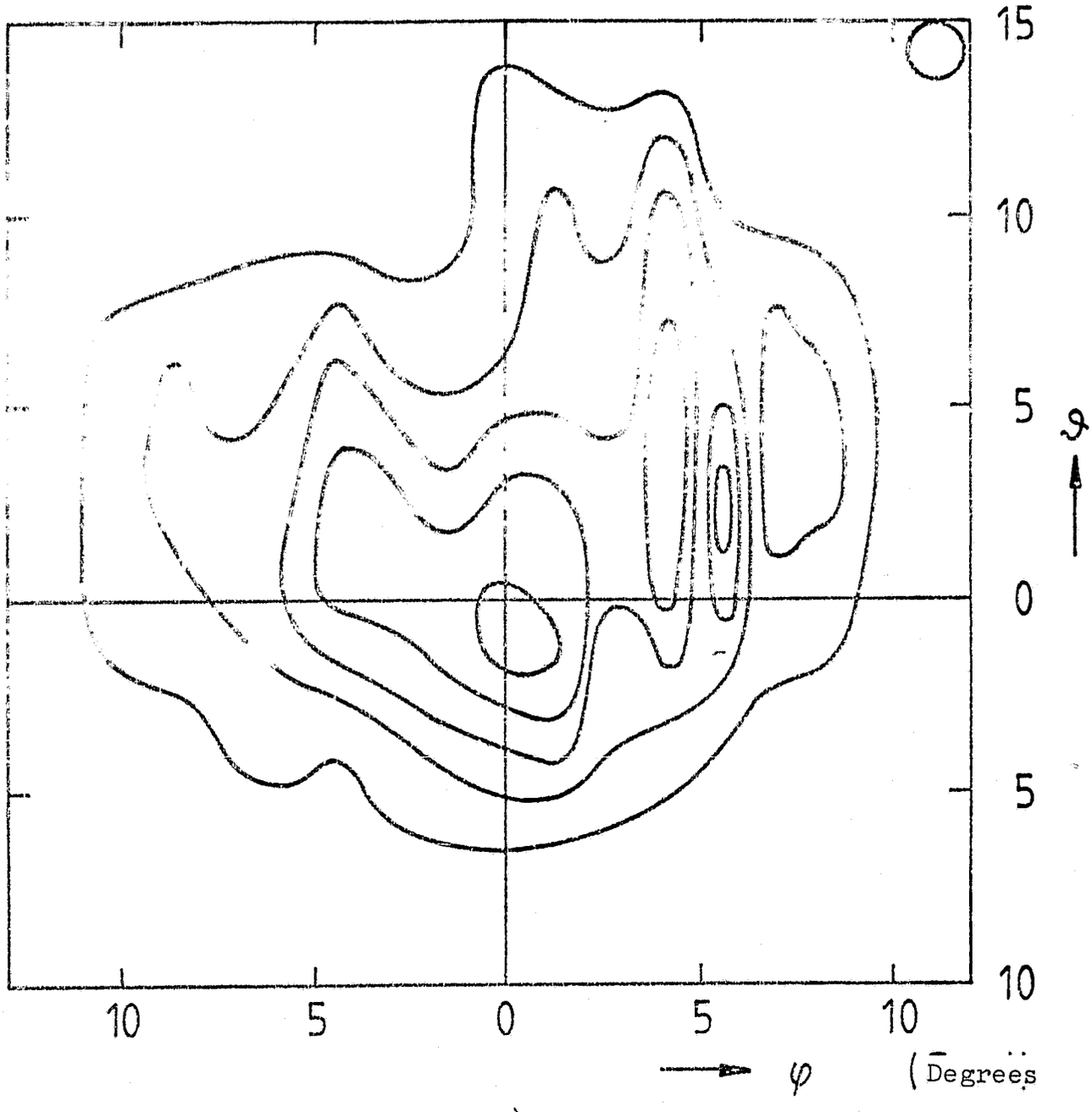

a)

Figure 22: Spatial intensity distribution in the beam bundle of the 4.4- μm diode at the working point 1.132 A (a) and at 120 mA (b) as well as of the 5.2- μm diode at working point 0.92 A (c). The relative radiation power is given by isophotes at fractions of the maximum value of 0.95, 0.8, 0.65, 0.5 and 0.35. The zero point of the angle scale is placed arbitrarily at the intensity maximum. The size of the 2 mm perforated lens and thus the spatial resolution is illustrated by a circle.

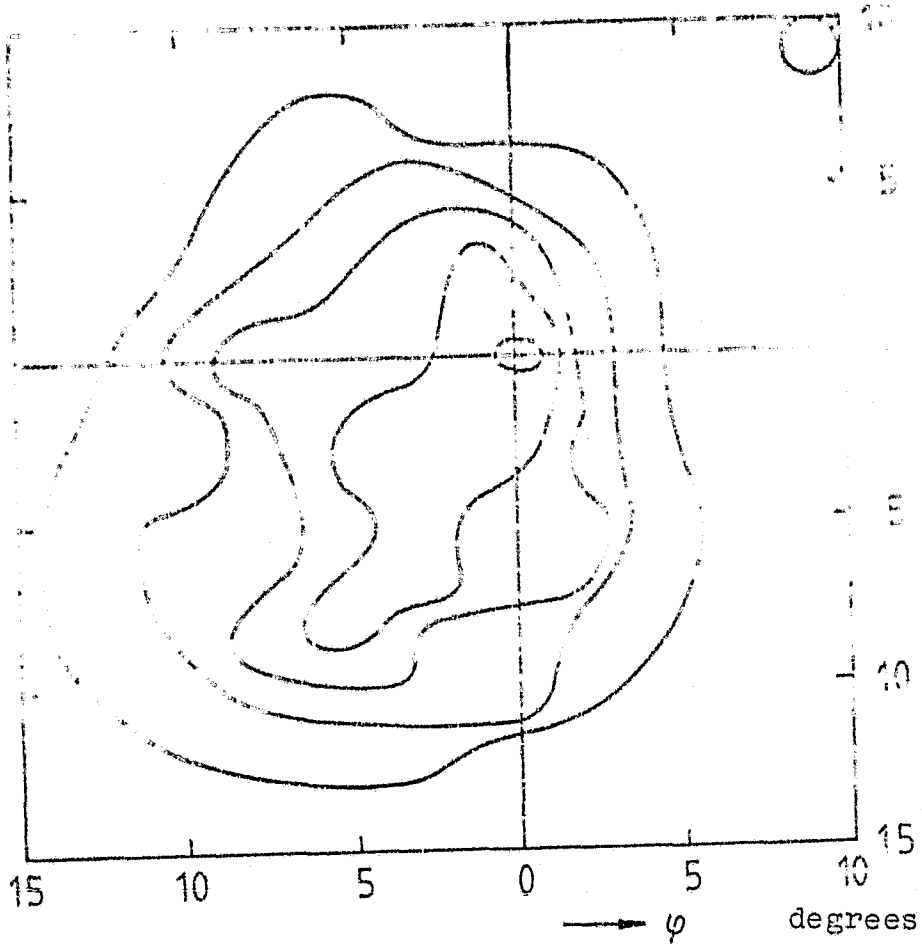

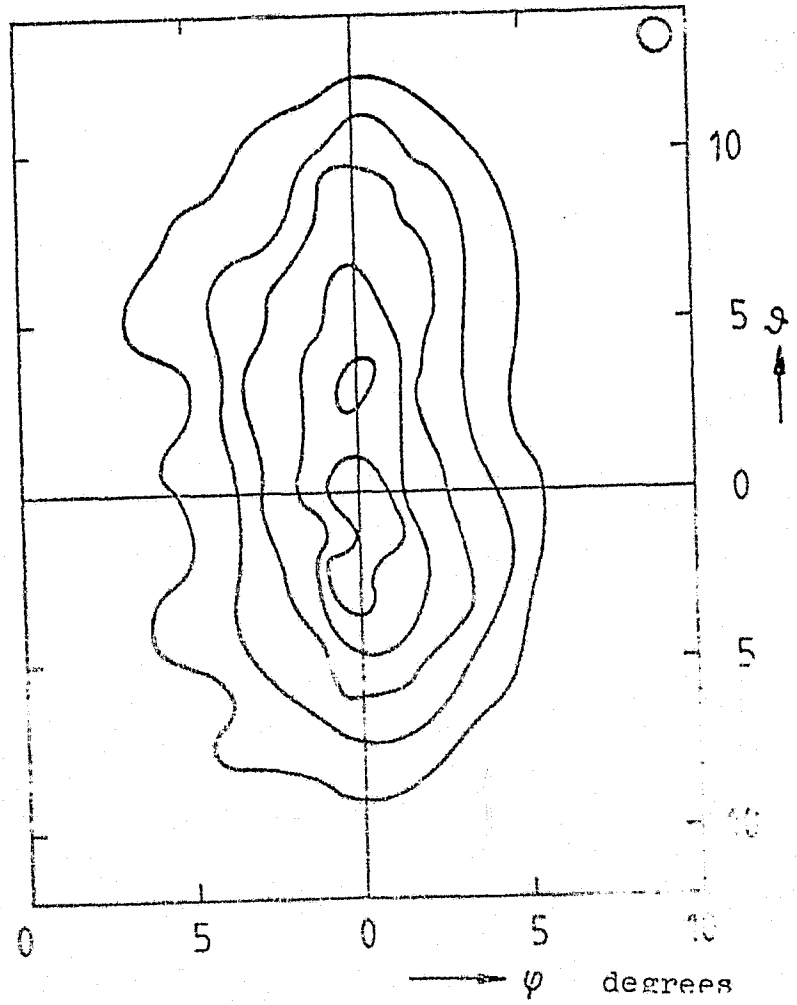

Figure 22

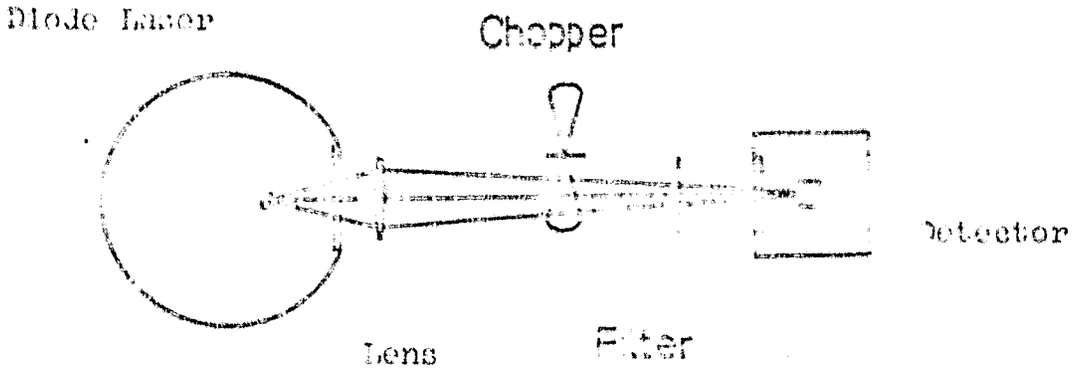

Figure 23: Sketch of the test setup to measure laser power

is of critical importance since it determines the resolution of the feed monitoring system for a given detector. An accurate measurement of the emission power output is very difficult to perform because of the bundle divergence and the severe background emission in the IR range. The available IR detectors posess sensitive surfaces of a few square millimeters. Therefore, the laser beam is imaged onto the detector by a Germanium lens (anti-reflects coated, focal length f = 38 mm). Transmission of the lens was determined as 0.83 at a wavelength of 4.4 µm and 0.96 at a wavelength of 5.2 µm by using a grid spectrometer (Perkin-Elmer), which is calibrated for plane samples, i.e. the given values represent lower limits. Since the laser power output at higher diode currents considerably exceeds the measurement range of the Golay detector used, an attenuation filter of black PE of 2.0% transmission was placed in front of the detector. The sketch of the test setup is shown in Figure 23. The emission power output P follows from the detector output signal S, the responsiveness of the detector R and the transmission of the optic components t as:

$$P = \frac{S}{t \cdot R} \qquad (4.1)$$

Several important measured values of the diodes are given in the following table.

	Diode current near the threshhold of laser activity	Diode current at the midpoint of laser activity
	Diode current power	Diode current power
[illegible]	[illegible]	[illegible]
[illegible]	[illegible]	[illegible]
[illegible]	[illegible]	[illegible]

Measured values at working point are und[illegible]

Figure 24: Radiation power of the [illegible] diode in arbitrary units above the diode current

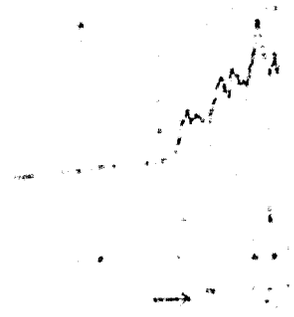

These values have been corrected so that they include that fraction of the beam bundle which cannont be imaged on the detector by the lens. However, the measurement errors due to inaccuracies in modulation of radiation were determined. A mechanical chopper invalidates the result considerably, due to its inherent radiation. On the other hand, a modulation through changing the diode current leads to instable operating conditions (see page 38, Figure 20), whereby larger measurement errors are also anticipated. The given values were determined by rectangular modulated current and agree within the error limits, with the values measured by using a mechanical chopper. The measurement is accurate to a factor of about two. The power output of about [illegible] measured at the working point of the 4.4-µm diode represents a good starting point for a high resolution feed modulation. /43

From the measured spatial intensity distribution, the laser power output can also be estimated. Because of the modulation of the emission by the diode current, this measurement exhibits approximately the same error as the measurement described above. The raster measured values define, analagous to equation 4.1, local emission power outputs P(ϑ,φ), from which we obtain a lower limit of total power output by using the following equation:

$$[illegible] = \frac{\Omega_R}{\Omega_B} \cdot \Sigma P(\vartheta,\varphi) \qquad (4.2)$$

(Ω_R: space angle of the raster element, Ω_B: space angle to the detector apperture, always with respect to the location of the laser)

This is true because there are no measured values available for the edge zones of the divergent bundle. The result of [illegible] agrees with the above value within the limits of acceptable error.

Through constant time changes of the diode current, the qualitative dependence of emission power output on the diode current was measured. It turns out that for all lasers an increase in power output occurs upon increasing the current, however, the relation between the two quantities is not always linear. This is illustrated by the example of the [illegible] diode in Figure 24. This measurement was performed with collimitered beam bundles, discussed in Section 5.1. /44

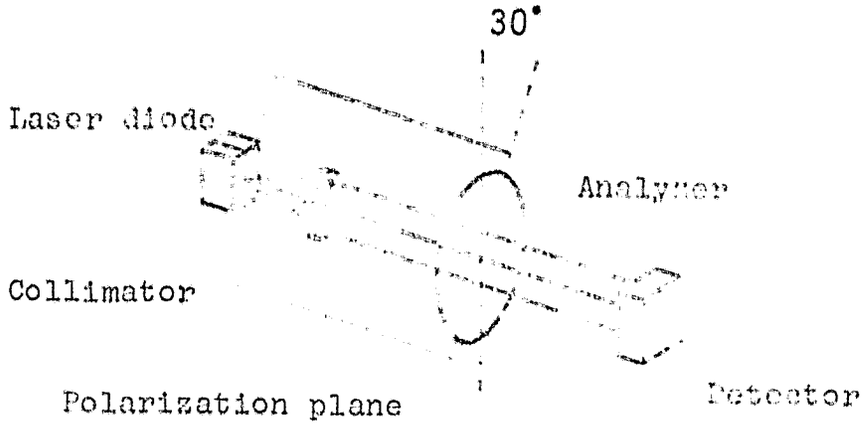

Figure 25: Sketch of the test setup with position of the polarization plane for vertical oriented p-n-transistion

4.1.6 Measurement of Polarization of the Laser Beam

Polarization of the referenced beam is important in connection with the efficiency of the beam splitter (Section 3.3). For radiation polarized perpendicular to the incident plane, the beam splitter achieves its maximum effectiveness. To measure the polarization, a grid polarizer is installed in the beam path of collimitered beam bundle as an analyzer and the transmitted intensity is measured as a function of the analyzer direction (Figure 25). At the working point of the 4.4 μm diode (0.959 A) a polarization degree of about 60% was found. The polarization plane is inclined 30° (measured counterclockwise) to the plane of the p-n-transition.

4.1.7 Measurement of Power Loss /45

For use in the helium cooled Michelson interferometer on GIRL, a power loss of less than 200 mW is permissible. Therefore, the vaporization rate of helium was measured in laboratory cryostats with the laser both on and off (4.4 μm diode) and the power loss was determined from this. The vaporizing helium gas was diverted through the bellows gas counter where it had a temperature of 25° C. After about 15 minutes the volume of vaporized gas with laser shutoff was 175 ± 2 l, with operation of the diode at the working point (0.959A), the volume was 320 ± 2 l, and after switching off the diode current, the volume was 180 ± 2 l in a control measurement. The vaporization rate caused by operation of the laser is thus $V_1 = 0.158 \pm 0.007$ l/sec at a temperature $T_1 = 25°$ C and air pressure $p_1 = 960$ mbar. If we convert this quantity to normal conditions ($T_o = 273$ K, $p_o = 1013$ mbar), then the vaporization rate becomes $V_o = 137 \pm 6$ cm³/sec.

Using the conversion factor between volume of gaseous helium at 273 K and the volume of liquid helium of the same mass at the boiling point (4.2K) $V_g/V_f = 699$, the density of liquid helium at the boiling point $\rho_f = 0.1248$ g/cm³ and the heat of vaporization L = 20.91 J/g, the power loss of the laser results as 0.51 ± 0.02 W from the following

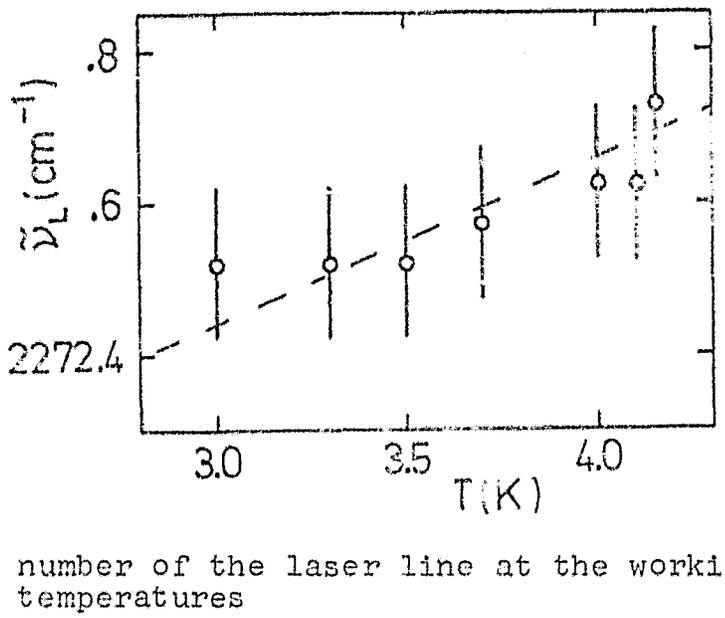

Figure 26: Wave number of the laser line at the working point 0.959 A for several bath temperatures

equation:

$$P_V = V_f / N_E \cdot L \cdot \varrho \cdot \dot{V}_c \qquad (4.3)$$

Since the voltage drop at the crystal cannot be measured during operation, the power loss from the voltage drop at the power feeds was estimated outside of the cryostat as a check on the above value. Because of the contributions due to resistances and numerous contacts, a value determined in this manner represents an upper limit. From the voltage drop of 0.75 V measured at the working point, a value of 0.72 W is calculated.

Because of the high power loss the tested 4.4-µm diode is not suitable for use on GIRL. Because of the good spectral properties and sufficient emission power, this laser can be used for the laboratory tests of the feed monitoring system. Conversations with the manufacturer had shown that laser diodes with the desired characteristics are also available for losses of 200 mW, but a suitable selection /46 process among the large number of diodes is needed. This work is currently underway.

4.1.8 Determination of the Thermal Wavelength Shift

By reducing the vapor pressure above the vaporizing helium, the bath temperature was reduced in steps to 3.0K and the spectrum of the laser at the working point was taken. The wave number determined in this manner as a function of bath temperature is shown in Figure 26 as it was determined from the changing pressure values. From this results an average shift in the laser line of about 0.2/cm/K.

4.2 The IR Detector

4.2.1 Detector Principle

A detailed discussion of the types and characteristics of detectors for IR radiation is found in Hudson, Hudson (1975). As a measurement effect, the thermally induced change in material properties is used for a certain group of detectors (e.g. temperature independence of electrical resistance for the Bolometer or of pressure for enclosed gas quantities in the so-called Golay detector). Another group uses quantum effects (e.g. generation of charge carriers in semiconductors). These effects cause an electrically detectable signal S to be formed from an incident emission signal P. Detectors using the thermal effect are generally much slower (response typically >1 msec) than quantum detectors (response time typically <1 μsec). One problem in the detection of IR radiation is the IR background radiation which falls into the detector in addition to the the desired radiation. In order to be able to detect weak intensities in front of a strong background, the radiation to be measured must be periodically chopped. The resulting intensity fluctuations then lead to a corresponding, periodic signal at the detector output which was usually independent of the background noise. The photon noise of the background radiation is now superimposed by the noise generated in the detector itself. Frequently, the manufacturers call the emission power output equivalent to the total noise voltage of the detector black background radiation at a given temperature. Photon noise of the background as well as internal detector noise are dependent on temperature, so that through reducing the temperature, the detection limit of the detector can generally be decreased. To measure astronomic IR radiation from very weak sources, the cooling of thermal detectors to less than 1 K is desireable (Katterloher 1978). Operating temperature of [illegible] in the GIRL interferometer is tuned to the expected astronomic radiation flux. To record the position interferogram with the desired S/N ratio, these low temperatures would not be needed.

Different detectors were tested for use at GIRL operating temperature. Responsiveness in the reference beam and detectivity were determined or the data from the manufacturer was checked. Measurements were performed on four detectors: three photo conductors made of copper dosed Germanium (Mullard Ltd., London; Advanced Kinetics, Costa Mesa, USA--two samples; operating temperature, 4 K) and one photo diode (InSb,, Barnes, Stamford, USA, operating temperature 77 K). Photo conducting detectors consist of one pure, one dosed and one connecting semiconductor. With copper dosed Germanium for instance, electrons of the foreign atoms are usually elevated by incident photons over an energy gap E_g into the conductivity band. The minimum excitation energy E_g of a semiconductor defines a limit wavelength $\lambda_g = hc/E_g$ (h: Planck constant, c: speed of light). Radiation whose wavelength exceeds this limit cannot be detected by the detector. The spectral sensitivity $R(\lambda)$ is therefore terminated at λ_g. With increasing photon energy, the responsiveness (generated charge carrier per incident power) decreases again since the number of charge carriers is proportional to the number of photons, so that a relatively narrow band sensitivity range results. A photovoltaic detector is designed as a semiconductor diode (detector used consists

/48

of indium antimonide). The same excitation mechanism and a similar response characteristic as the simple photoconductor is found here. The charge carrier pairs generated by absorption of the light quantum are separated by the diode in the field of the charge carrier zone. Thus, a photo-voltage is generated which is proportional to the incident emitted power. The properties of the detector depend considerably on the applied bias: by means of an additional controllable counter-voltage, the detectivity can be optimized. With photoconductors however, only through the application of an external bias can an electrical signal be obtained. Figure 27 shows the circuits used to connect the detectors to the preamp input. Already tested amplifiers with known frequency response and noise factor were used.

4.2.2 Measurement of the Responsiveness /50

Determination of the responsiveness R of the detectors is used to precalculate the signal generated by the laser interferogram, and to determine the noise equivalent power according to Equation 3.16. Since no calibration source was available, the Golay cell was used as a reference since accurate information on the responsiveness as a function of wavelength and chop frequency was made available by the manufacturer. This thermodetector consists of a radiation absorber and a connected gas cell with diaphragm. Under the effect of IR radiation the gas in the cell heats up. Due to the resulting increase in pressure, the diaphragm is pressed into a wall of the cell: this is converted into an electrically measureable signal. The sensitivity range extends from visible light down to submillimeter wave radiation. However, it is limited by the entrance window (to a wavelength range between 1 and about 50 µm through a KRS5 window in this detector). The time constant of this detector is about 1 second.

Since the responsiveness of the detectors at the reference wavelength is of interest, a semiconductor diode laser was always used as emission source. From its cone of rays, a bundle was generated through a perforated aperture which was measured by the Golay detector and by the detector under study. Selection of the aperture is governed by the different size of the detector element. The bundle must have sufficient cross-section so that it can still be fully registered by the detector with the smaller sensitive surface. By means of a lens, the divergent laser beam bundle is collimitered at the detector to achieve sufficient emission power outputs (Figure 28). The sensitivity of the Golay cell is in principle high, depending on the chop frequency; a favorable frequency range is between 0.2 and 20 Hz. Therefore, the laser radiation is chopped by the 13 Hz modulated diode current of the laser supply system. Here, the responsiveness according to the manufacturer is $R_0 = 1.7 \cdot 10^6$ V/W, that is, 74% of the maximum value at 1.5 Hz. The electric detector signal is measured by a lock-in amplifier (Ithaco, Mod. Dynatrac 391A). Because of the method of operation of the lock-in amplifier (phase sensitive rectification of the signal base wave), the indicated value depends on the feed signal shape. Because of the different response times of the detectors, different signal shapes are produced and this leads to uncertainties of up to 10% in the signal amplitude even after appropriate correction. A read-off of the signal from the oscilloscope is /51

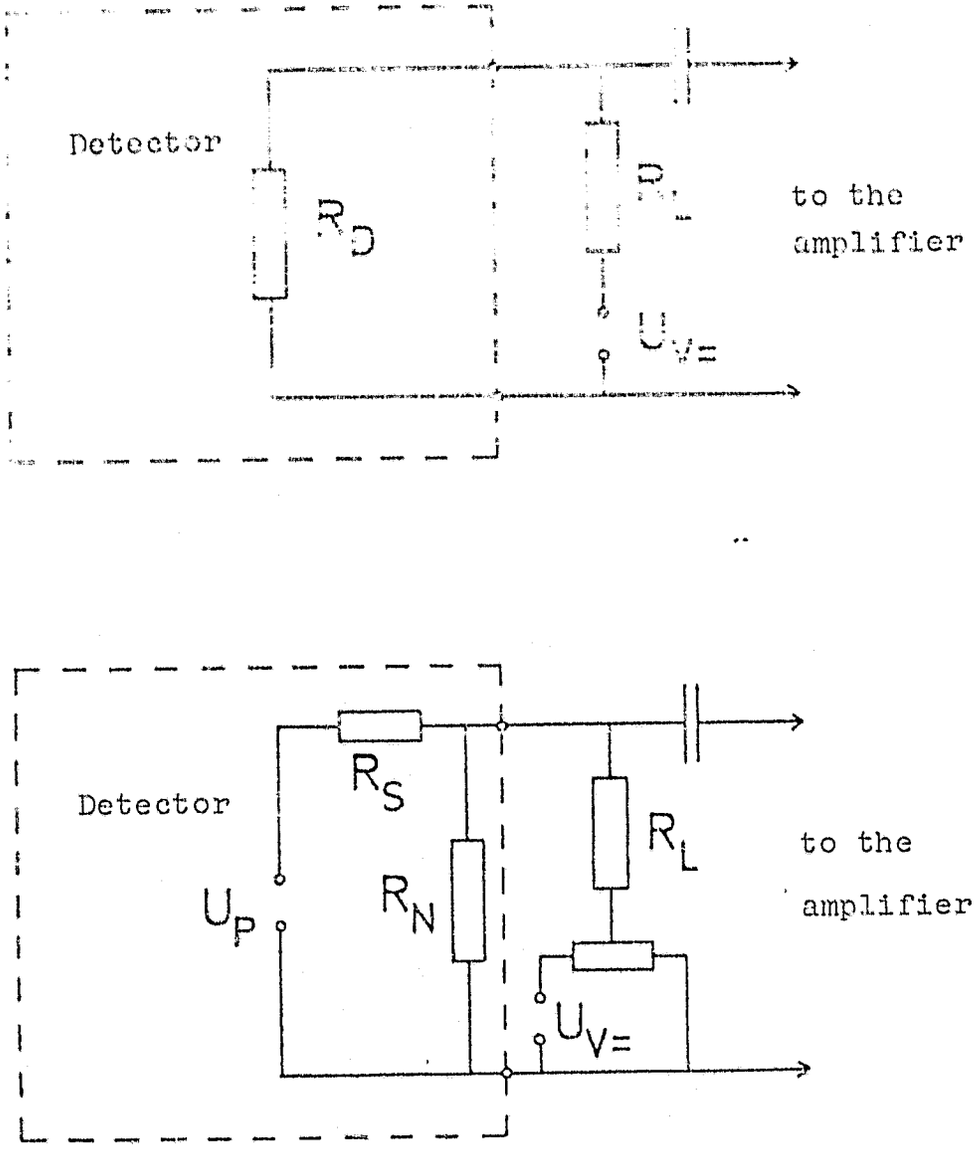

Figure 27: Block diagram to connect the IR detectors to the preamplifier.
a) photoconductor
R_D: radiation dependent resistance (detector element)
U_V: supply voltage, R_L: load resistant
b) Photodiode
U_P: radiation dependent photo voltage, R_S, R_N: series and shunt resistance of the diode (simplified substitute diagram). A controllable countervoltage can be applied by means of the d.c. source (U_V).

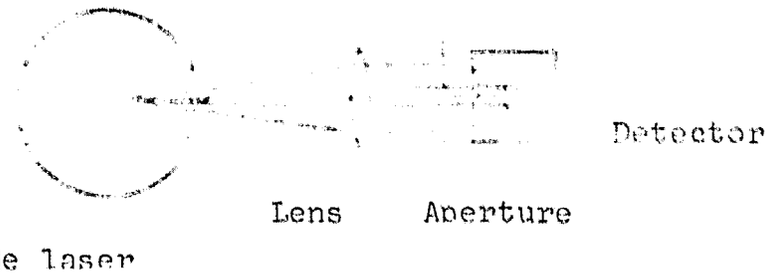

Figure 28: Sketch of the test setup for comparative measurement of the response capability

not very accurate because of the large, effective bandwidth.

The sensitivity of the quantum detector itself depends very little on the chopper frequency. Therefore, for a frequency of the interferogram signal of about 80 Hz, only the smallest deviations in the responsiveness from the values determined at 13 Hz is expected. A comparison measurement at 80 Hz is not possible because of the significant loss in sensitivity of the Golay detector. For different laser power outputs, the signal voltages of the Golay cell S_o and of the detector to be studied S were measured and, by using the equation:

$$R = R_o \cdot \frac{S}{S_o} \qquad (4.4)$$

the responsiveness R related to the Golay detector was calculated. The signal ratio S/S_o is not entirely independent of the selected radiation power in several cases. The cause for this is a deviation in the relationship between output signal and incident radiation power from a linear function. In this case, the signal values corresponding to the size of the expected interferometer signal (at about [illegible] μW) are considered. Most values of responsiveness were taken at a laser wavelength of [illegible] μm and these are given in the following table, together with data from the manufacturer.

The deviations from experimentally determined values are partly due to measurement uncertainties, absorption by the entrance window (the resulting responsiveness with the rigid window cannot be determined exactly because no transmission data are available), by the special test conditions (instead of a black body emission, monochromatic radiation is measured) and by alteration effects in a detector (Mullard). The greater responsiveness of the Golay detector is based on the amplifier integrated into the detector, whereas the other values contain no amplification factors. /52

For laboratory testing of the feed monitoring system, a 4.4 μm laser (SDL, Laser Analytics Company) and the InSb detector were used. Since this detector has its maximum responsiveness at [illegible] μm), the

Detector type	Response Capability Manufacturer's Data at	Measured Value at
[illegible]	[illegible]	[illegible]
[illegible]	[illegible]	[illegible]
[illegible]	-	[illegible]
[illegible]	-	[illegible]
- cell	[illegible]	Reference

Data from the manufacturer relate to a wavelength of 5 μm and were obtained by conversion of the maximum sensitivity (usually supplied) with the supplied sensitivity characteristics.

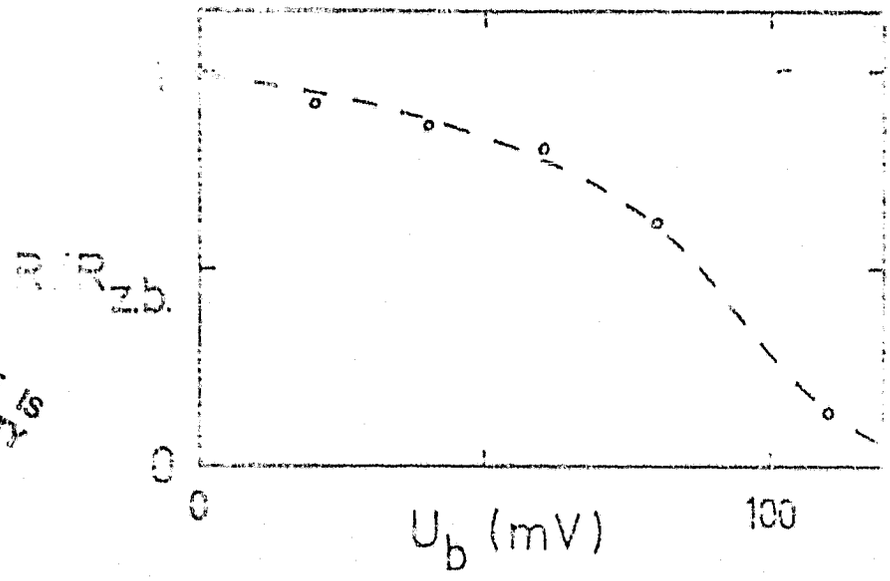

Figure 29: Relative response capability $R/R_{zero\ bias}$ as a function of the diode bias voltage U_b

responsiveness at 4.4 μm ($1.2 \cdot 10^4$ V/W) is much greater than at 5.2 μm ($2.1 \cdot 10^3$ V/W); the values indicate the steep drop in sensitivity near the boundary wavelength. These values were determined at a "zero bias," that is, the countervoltage was adjusted so that the photovoltage $U_p \simeq 109$ mV caused by the laboratory background (ca. 300 K) was completely compensated (zero bias condition). By variation of the countervoltage at constant emission signal, the relationship between responsiveness and the bias applied to the detector (diode bias voltage) was determined. Figure 29 shows this relationship. The best responsiveness is achieved for declining bias without adjustment

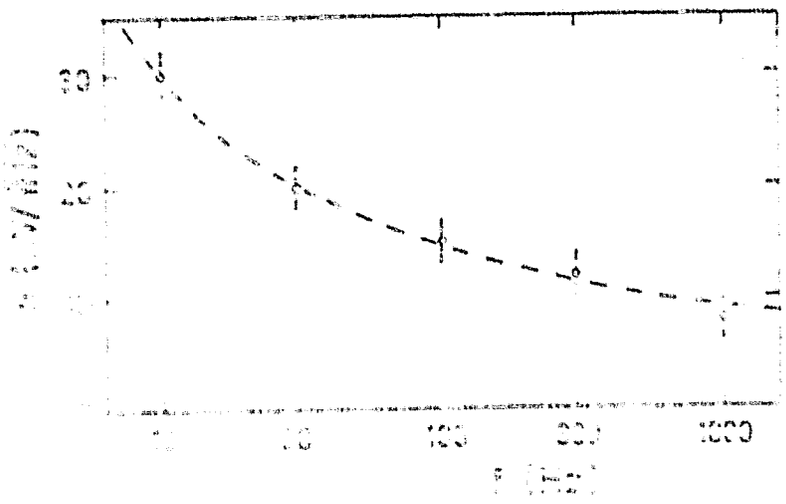

Figure 30: Relationship of noise voltage n with frequency f for the InSb detector

of the photovoltage, a regression to 15% of the maximum value is found.

4.2.3 Determination of Noise Equivalent Power (NEP) /53

One important criterion for selecting the particular detector is the noise equivalent power, since it is in a direct relation with the S/N ratio of the interferogram point and thus with the reading accuracy. From the measured values of the responsiveness R and the noise voltage n of the detectors, according to 3.16 the NEP can be determined. To measure the effective value of noise voltage, a lock-in amplifier with a noise option was used (Mod. Dynatrac 391A, Ithaco Company). Thus, noise spectra could be measured in the frequency range between 10 Hz and 1 kHz with variable bandwidth. With a variable bandwidth of 1 Hz the standarized noise level n can be read off immediately. The detectors were operated under conditions where the sensitive element is exposed to the unchopped laboratory background of about 300 K. Because of the greater background noise at this temperature compared to GIRL conditions, the measured detectivities are smaller than at 4 K background temperature. The potential improvement is insignificant however, since internal detector noise still predominates: the amount of photon noise contained in the background emission for known emission power output P_H and temperature T_H of the background amounts to a maximum

(Katterloher 1978). As a initial rough estimation for the InSb detector we have: with the effective background radiation of about /54 for a given sensitivity range and given Etendue at the sensitive element, there results a noise level of

whereas the given NEP is greater by a factor of 5. In the frequency range of the lock-in amplifier, the noise voltage was measured with a bandwidth of 1 Hz at several frequencies. With increasing frequency a drop in noise voltage shows up. This is illustrated in Figure 30 for the photovoltaic InSb detector. The decline in the curve is attributable to so-called 1/f noise contributions (Hall et al. 1975). When using the preamplifier for these measurements (Infrared Laboratories Inc., Tucson, USA), an upper limit frequency of the entire circuit of more than 10 kHz results. Through extrapolation up to 10,000 Hz (integration time of the position electronic system, Section 2.2) while retaining the value measured at 1,000 Hz (worst case), the average effective noise voltage n can be estimated for the interferogram. Thus, from Equation 3.16 we obtain the noise equivalent power as:

$$NEP = \frac{n}{R} \qquad (4.5)$$

or the detectivity as $D = NEP^{-1}$. The measured NEP values are given in the table below together with the values provided by the manufacturer.

Detector type	[illegible] NEP		[illegible] NEP	
	Manufacturer's Data	Measured Value	Manufacturer's Data	Measured Value
[illegible]	[illegible]	[illegible]	[illegible]	[illegible]
[illegible]	-	[illegible]	-	[illegible]
[illegible]	[illegible]	[illegible]	[illegible]	[illegible]
[illegible]	[illegible]	[illegible]	[illegible]	[illegible]

Since the NEP is also independent of wavelength--just like responsiveness--the manufacturer's data must be converted to the reference wavelength. Here, an error of about 20% is expected. Deviations of measured values are partially due to inaccuracies in the determination of noise voltage, and partly due to errors of measured values of responsiveness.

The maximum permissible NEP in the reference beam at a power output of 10 [illegible]W is $5 \cdot 10^{-11}$ W/ $\sqrt{Hz}$ (see Section 3.2). Therefore, the first two photoconductors checked at operating temperatures of 4 K are unsuitable for the position interferometer. The S/N ratio when using the Advanced Kinetics (AK) detector is calculated as about 20 from equation 3.17, this was also estimated in a corresponding test with a laboratory setup of the feed monitoring system on an oscilloscope.

To set up and test the system in the laboratory, the photovoltaic

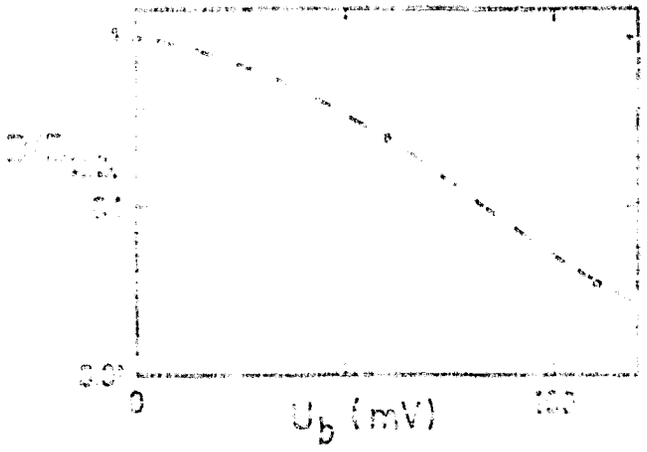

Figure 31: Measured dependence of the standarized detectivity $D/D_{zero\ bias}$ of the InSb detector on the bias voltage U_b

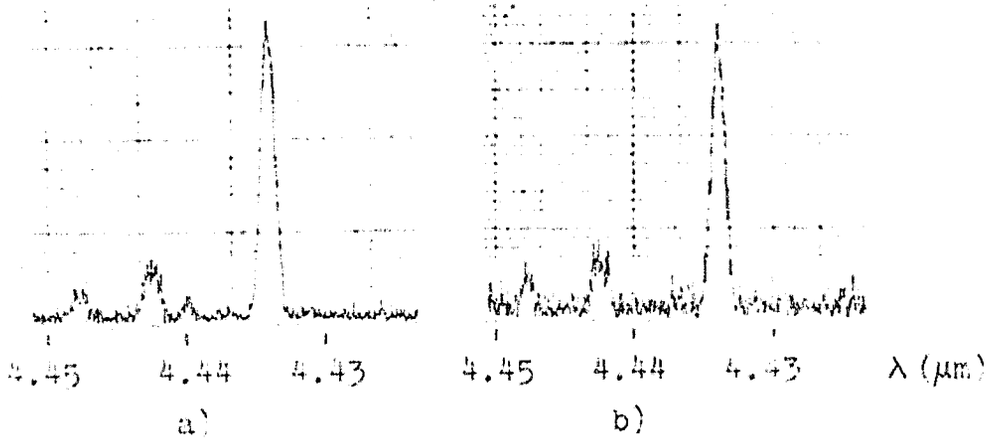

Figure 32: Spectrum of the ~4.4-μm diode at 144 mA
a) detector was driven under optimum conditions
b) operation at bias of ca. 20 mV

InSb detector was used. The required S/N ratio of 800 (see Section 4.4) can be achieved with it even with a power output less than 1 μW in the parallel beam. The noise of this detector is dependent on the bias declining at the detector element. Thus, with the profile of responsiveness already shown there follows a regression of detectivity with increasing bias (Figure 31). The best properties are found for the detector thereafter at 0 bias conditions; the detectivity given in the table was obtained with this mode of operation. Likewise, under this optimum condition, the detector was now operated for all measurements. A deviation from this condition led to an increase in noise in the signal emitted by the detector. This can be demonstrated for example, by using two laser spectra taken at very low laser power, one at zero bias and one with non-zero bias (Figure 32). With the

second spectrum, an increase in noise is seen.

The detectivity of the InSb detector also depends on the intensity (see manufacturer's information) of incident radiation of wavelengths < 1 μm, provided they encounter the sensitive element during cooling to 77 K. The NEP value ($1 \cdot 10^{-12}$ W/ [illegible]) was measured after covering the detector with a Germanium lens (transmission only for $\lambda > 1$ μm) during the cooling phase. Without covering, the value is about $1 \cdot 10^{-11}$ [illegible]. However, once the detector reaches its operating temperature the radiation remains below 1 μm without adversely affecting the detectivity. /57

4.3 Beam Splitter--Determination of Efficiency

Through the measurement of reflection and transmission on available mylar foils 5.0 ± 0.5 μm and 12.0 ± 1.2 μm thick (manufacturer's data), the efficiency was determined experimentally and suitability of the foils for the Michelson interferometer, specifically for laboratory setup, was checked. The accuracy of the thickness information is not sufficient to determine applicability of the foils at the wavelengths of λ = 5.2 μm or 4.4 μm by using the equations in Section 3.3. Therefore, phototransmission and reflection of unpolarized light was checked with a spectrophotometer (Perkin-Elmer Company). The measured results are shown in Figures 33 - 35 and are discussed below.

The strong absorption lines in the region between 5 and 14 m affect reflection and transmission decisively and render mylar useless as a beam splitter in this spectral range. The periodicity is explained by the Term cos δ in equation 3.20. With equation 3.22, the foil thicknesses are determined as 4.8 ± 0.1 μm from the spectral separation of the reflection maxima or transmission minima. For an angle of incidence of 45° in the interferometer, we thus obtain favorable wavelengths from equation 3.22 as λ = 29.9, 9.5, 5.7, 4.1, 3.2, 2.6 μm, which roughly agrees with the position of the transmission minima measured at a 45° angle of incidence (Figure 34). The deviations can be attributed to inaccurate knowledge of the refractive index which affects the period of reflection and transmission, and to the phase jump of the reflected beam which is different for reflection at the outer and inner boundary of the foil (Dielectricum). In the ideal case (electrical conductor) this leads to an additional phase shift π between the inner and outer reflected beam, as contained in equation 3.20. A phase shift different from π causes primarily a shift in the r_o and t_o curves while keeping the periods constant.

The maximum efficiency in the shortwave range can be determined by the reflection maximum r_o = 0.15 and the transmission minimum t_o = 0.8 and amounts to 0.48. The absorption of the thicker 12 μm foil is clearly greater than that of the 5 μm foil. From the periodicity a full thickness of 12.2 ± 0.2 μm is found. The beam transmitted at 45° is partially polarized and results in a polarization effect in the transmission curve which is caused by the instrument.

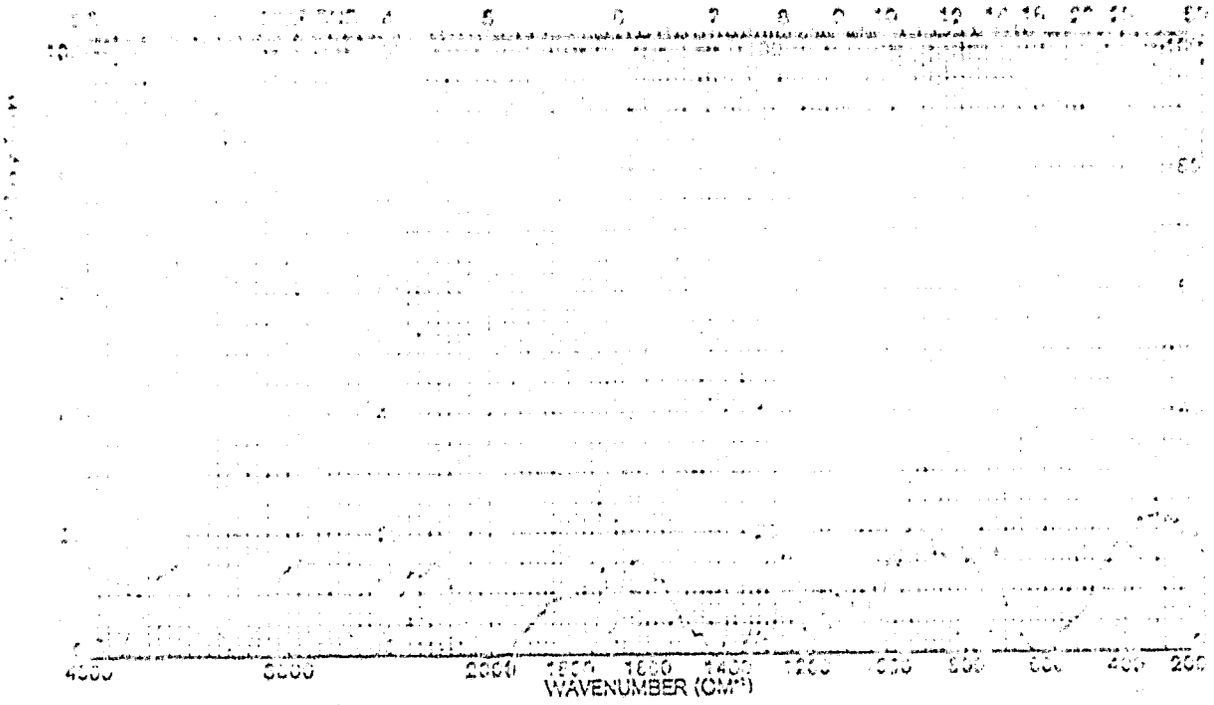

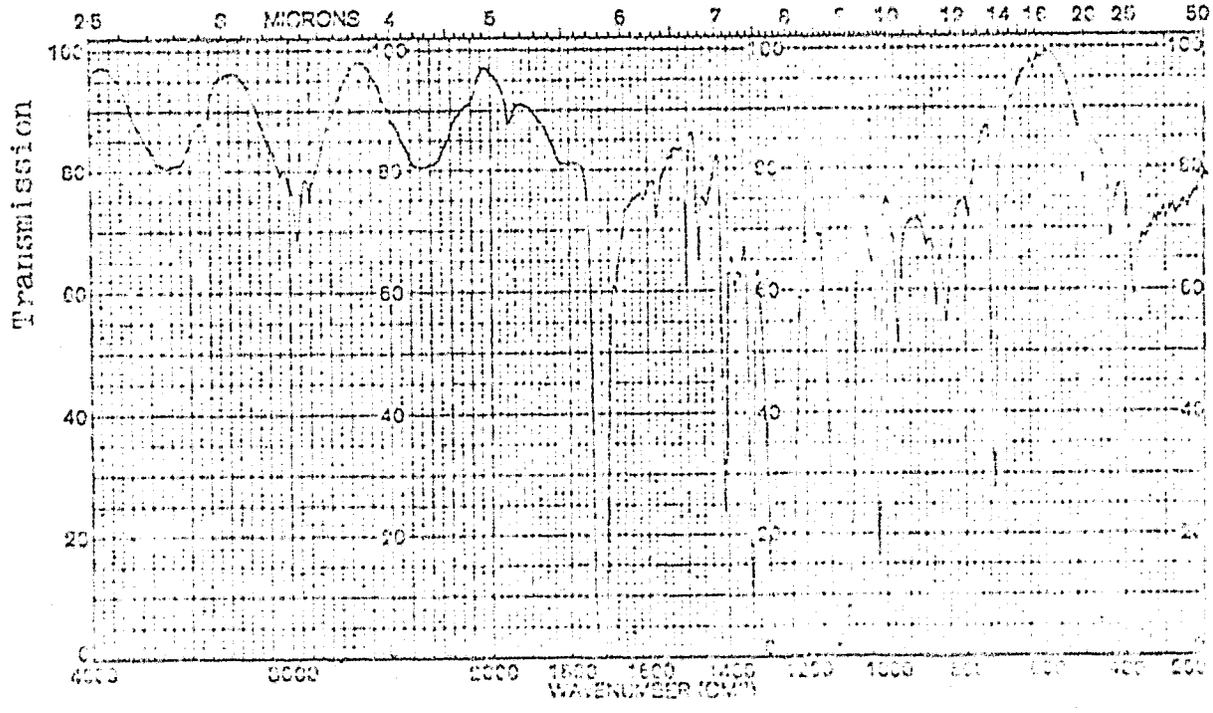

Figure 33: Reflection and transmission of the 5- ,m foil for perpendicular light incidence (angle of incidence upon reflection of 6.5 degrees is due to the equipment, it has only an insignificant influence on the periodicity of the curve).

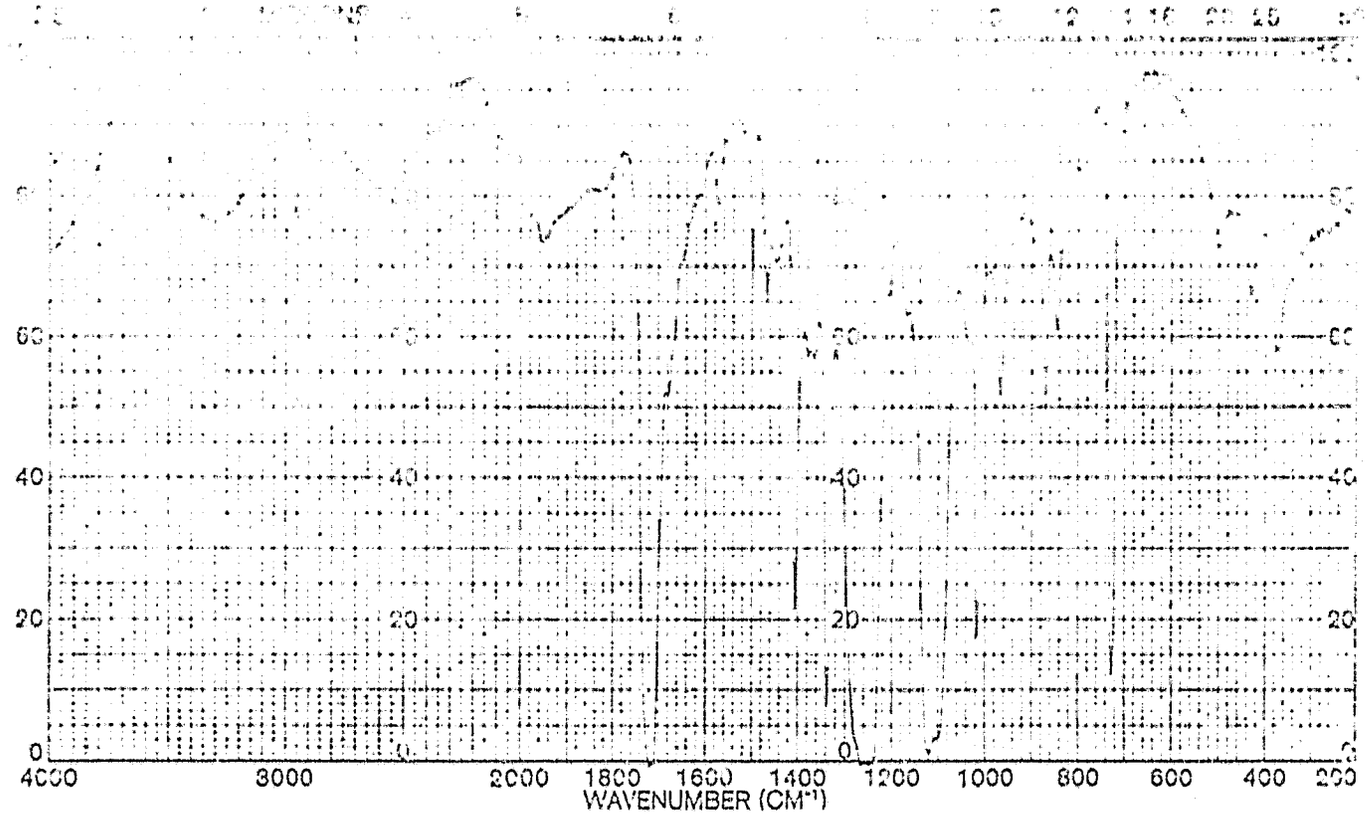

Figure 34: Transmission of the 5- μm foil at 45° angle of incidence.

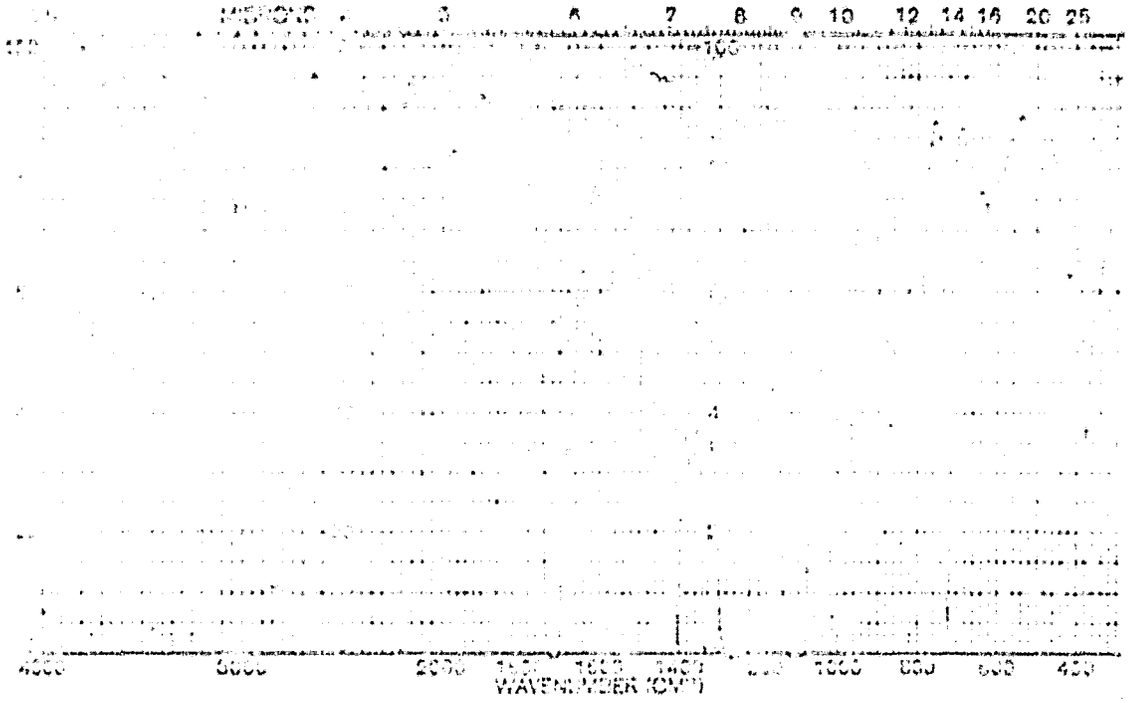

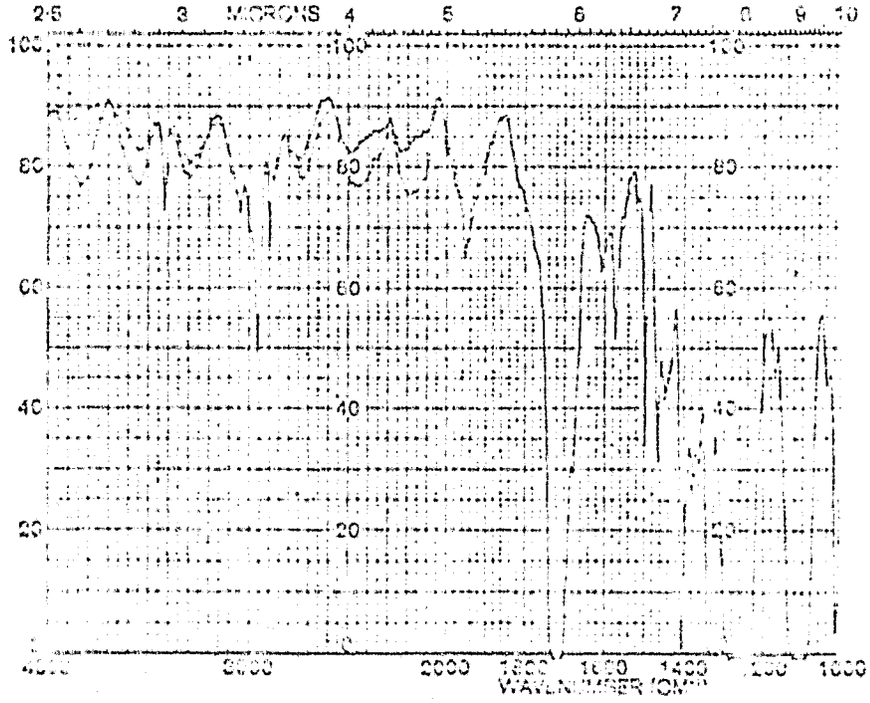

b)

Figure 35: Transmission of the 12- μm foil for perpendicular light incidence (a) and for 45 degree angle of incidence(b) for vertical and horizontal alignment of the incident plane

By means of recording the transmission spectrum using perpendicular polarization planes--achieved by suitable positioning of the foil--this effect was quite visible (Figure 34b). /62

Recording the reflection spectrum at an angle of incidence of 45° is not possible. From the transmission curves the favorable spectral ranges can also be read off to show where the transmission minimum is found. Both foils accordingly have a good effectiveness at 5.2 μm, at the wavelength of the laser used (4.4 m) however, they have a very small effectiveness. With the radiation of this laser, the entire transmission and reflection of the 5 μm foil at an angle of incidence of 45° is now determined. The diode was inserted in the cryostats so that the plane of the p-n transition was perpendicular to the incident plane of the reference beam in the interferometer. The polarization plane of the laser (Section 4.1.6) was thus sloped only 30° to the favorable vertical polarization direction where the maximum efficiency values are achieved. The reflected power of a collimiter laser beam was 2%, the transmitted power was 98% of the incident power. Thus, an effectiveness of 0.08 results so that when using a beam power output of 10 μW at the detector with the measured NEP (10^{-12} W/$\sqrt{\text{Hz}}$ from Equation 3.17, a S/N ratio of 4,000 for the interferometer signal is obtained. Thus, this beam splitter can be used for laboratory tests with the 4.4 μm diode.

4.4 Test of the Positioning Electronic System /63

The positioning electronic system was developed by electrical engineers at the institute and is described in Appendix 2. Below we shall report on the tests performed with it. In order to do this, the laser interferogram was simulated by voltage signals. Using a sine signal with a frequency of 80 Hz, a non-interferred interferogram was generated in order to study the influence of signal amplitude on the behavior of read pulses belonging to extremal and zero positions. The time shift between attainment of the extremal position and transmission of the appropriate pulse was on the average 2τ for a maximum amplitude of 5V; (τ : integration time of the position electronic system, see Section 2.2) and this was increased upon decay of the amplitude below 1.5 V. The corresponding shift between attainment of the zero position and the transmission of the read pulse (at maximum amplitude, equal to τ on the average) increases upon decay of the signal amplitude below 0.2 V. Thus, the actual signal profile at the detector of the positioning interferometer with amplitudes between 3.8 and 5 V permits the use of all support points when utilizing maximum resolution.

The main interest of the test was devoted to the behavior of the read pulse with an interfered signal. Through periodic motion sequences of mechanical parts (e.g. crankless engine) as well as through statistically distributed interference (e.g. detector noise), the laser interferogram was modified. This was simulated by superimposing sine signals with discreet frequencies or noise voltages of different bandwidth on the undisturbed signal. The block diagram of the test setup is shown in Figure 36. By variation of the interference

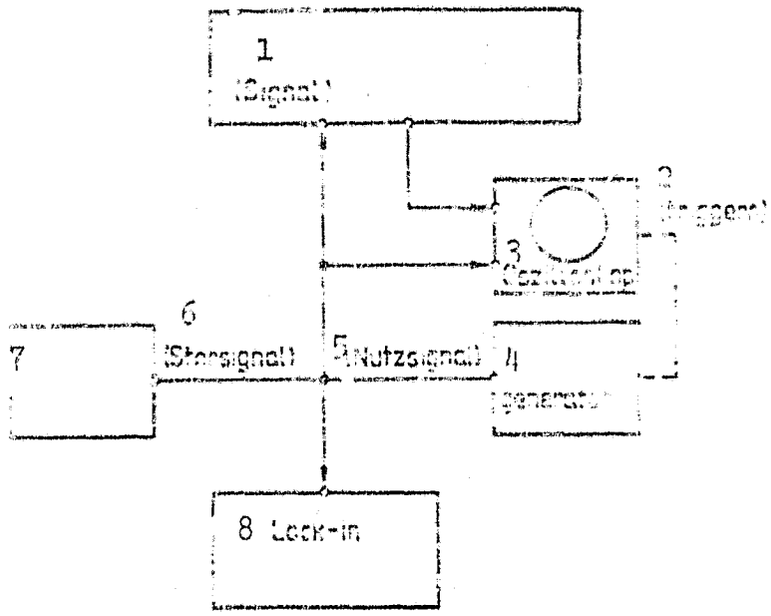

Figure 36: Block diagram to simulate the feed monitoring with disturbed signal

Key: 1-position electronics (signal) (readout pulse) 2-trigger 3-oscilloscope 4-sine generator 5-useful signal 6-interference signal 7-noise generator 8-lock-in amplifier

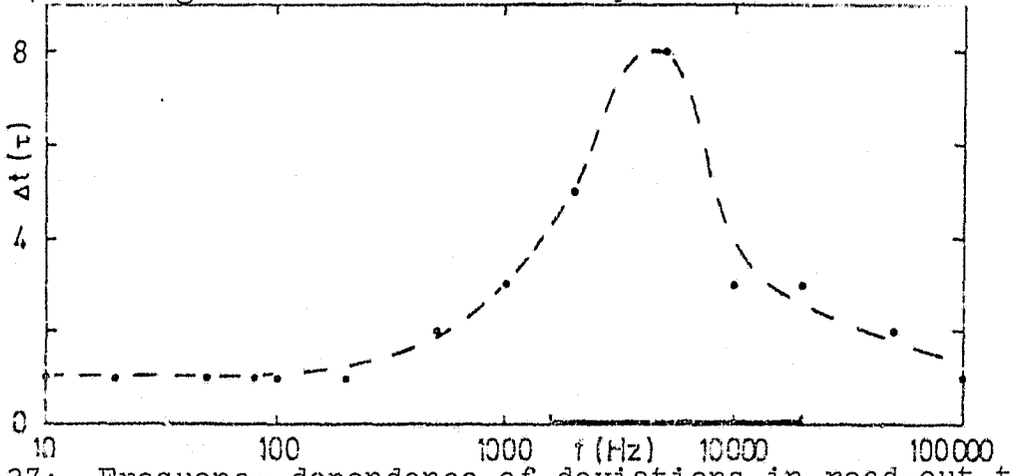

Figure 37: Frequency dependence of deviations in read-out time point for constant useful-interference voltage ratio 200 and the frequency of the useful signal 80 Hz.
Δt: time interval within which the pulses belonging to an extreme position are transmitted. The time interval between regular readout pulses is $32\,\tau$. Multiple pulses appear in the frequency range marked by the bar.

and useful voltages (the latter only within the permissible range), any signal to noise ratio or useful-interference voltage intervals could be achieved. With a lock-in amplifier (Dynatrac 391A, Ithaco Company), a control measurement of the noise voltage was performed. Fluctuations in the read time point were observed on the oscilloscope.

With increasing interference voltage, growing deviations in the read time point compared to the time point with pure signal and multiple pulses appear primarily in the region of the extremal point of the pure signal. Multiple pulses are generated in the immediate vicinity of ideal support points if the interference-induced signal fluctuations at the zero passages and at the extremum can be considered to be additional zero passages or pole to extrema from the viewpoint of the positioning electronic system. Since each value whose read was triggered by a pulse during transformation of the main interferogram is assigned to a discreet, ideal support point, multiple pulses invalidate the feed monitoring. /64

The interference susceptibility of the read time point is also dependent on the frequency of the superimposed sine interference (Figure 37). The greatest fluctuations resulted at frequencies between 1,000 and 10,000 Hz. The zero pulses under these conditions exhibit no time fluctuations. /65

The decisive quantity in the calculation of effects on the Fourier spectrum is the standard deviation of the pulse locations. This is obtained by assuming uniform distribution of the read time points from the actual observed shifts Δt_i and the average shift (Δt) compared to attainment of the ideal support point positions by using the equation:

$$\sigma_x = \frac{\dot{x}}{J} \sqrt{\sum_{i=1}^{J} \Delta t_i^2 - (\Delta t)^2} \; .$$

Here, the feed velocity is assumed constant. (J: number of different read times belonging to an ideal support point).

With sine interference of different frequencies, the dependence of the standard deviation σ_x on the useful-interference ratio S/N was studied. The typical behavior of the standard deviation for a low and a high jamming frequency is shown in Figure 38. When using all support points, the solid curves are obtained, when limited to the zero passages, the dashed curves illustrate the relationships. The time interval τ corresponds to the optic shift $\lambda_L/128$ (see equation 2.8), which is why the size of the standard deviation is proportional to the laser wavelength. The given values pertain to $\lambda_L = 5$ μm. It is clear that interference signals of high frequency must be better suppressed than low frequency signals in order to limit the support point error. When using the zero passages, a S/N = 1,000 ratio, standard deviations of less than 0.0.04 μm are obtained. Use of all support points requires greater interference voltage intervals and furthermore, the appearance of multiple pulses must be eliminated. This is achieved at 4,000 Hz with S/N $\geq$ 1,000. /66

Likewise, with noise interference of various bandwidths and

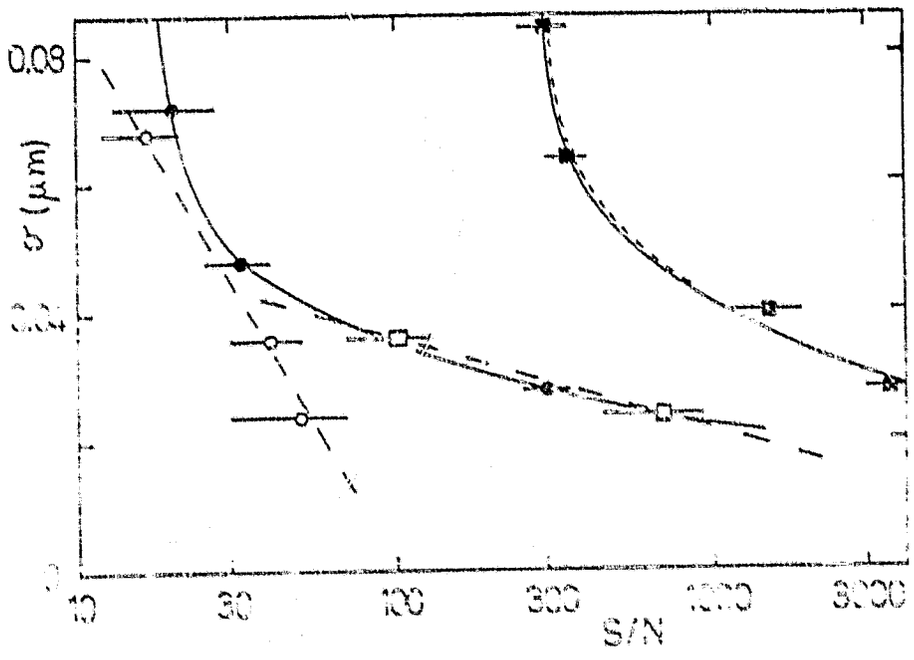

Figure 38: Standard deviation of support points of the function of useful-interference voltage ratio at frequencies of sine interference of 90 Hz O and 4000 Hz □. Auxiliary lines: appearance of multiple pulses

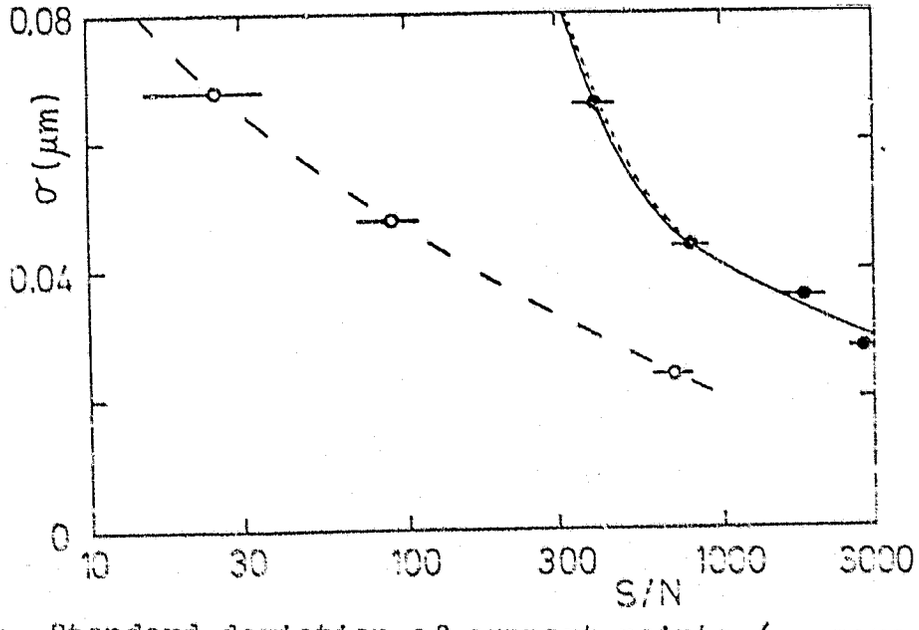

Figure 39: Standard deviation of support points (-- zero passages, —— all support points) as a function of signal to noise ratio at λ_L=5 μm for white noise of 10 kHz band width. Additional lines: appearance of multiple pulses.

nearly frequency independent voltage (white noise), the relationship between S/N ratio and the standard deviation of the support points was studied. Figure 39 shows the relationship when using the zero passages and all read points on the example of a detector-like noise with an effective bandwidth of the positioning electronic system (10 kHz). To maintain the permissible standard deviation of 0.06 m, the following minimum values of the S/N ratio are needed:

all support points: 800 (due to multiple pulses)
zero passage: 70.

Since the named interference increases the standard deviation in addition to the effects based on the spectral properties of the laser, in order to assure sufficient read accuracy, a higher S/N ratio than above is needed and a simultaneous limitation of the monofrequency interference(especially of higher frequencies) is required. Therefore, the exclusive use of zero positions as support points is expedient; because of the large number of support points (see Section 2.2) this does not result in a limitation in spectral resolution in the Fourier spectrum. /67

5. Assembly and Testing of the Feed Monitoring System /68

5.1 Description of the Laboratory System

The position interferometer consists of its specific components (diode laser, detector and positioning electronic system) and also uses the optic components of the main interferometer. Since the final launch version of the main interferometer was not yet available a laboratory model was constructed whose components are described below. As end reflectors in the interferometer arms, we used two gold vapor plated plane mirrors with surface irregularities less than 0.5 μm. To divert the partial beam in the moving interferometer arm, the cube corner intended for use in GIRL was used. It is mounted on a moveable table whose tip is less than the permissible value when using a cube corner (about 1^{0}). By means of tip measurements with a laser interferometer made by Hewlett Packard (Laser Measurement System, Mod. 5526A), tips of a maximum 13 arc seconds about a vertical rotation axis and a maximum three arc seconds about a horizontal axis were measured over the entire feed path of 25 mm (this corresponds to an optic feed path of L = 10 cm). At the micrometer screw of the adjustable table, a drive motor is connected by means of a spring bellows. Since the variations in the crankless engine in its present design resulted in severe interference with the jamming model, a low vibration d.c. motor (Dunkermotoren Company, Model GR 50x45) was used for the drive. Thus, a sufficient uniform movement of the cube corner was achieved. To attenuate external vibrations the interferometer was built on an air cushion optical bank (Vibration Isolation System, Ealing Company, South Natic, USA) whose internal frequencies lie in a range of 1 Hz--that is, far beyond the interference frequency range. The laboratory setup is shown in Figure 40. With the exception of the laser (operating temperature 4 K) and the detector (77 K), all components of the system were at room temperature.

For use in the feed monitoring system, the divergent laser beam

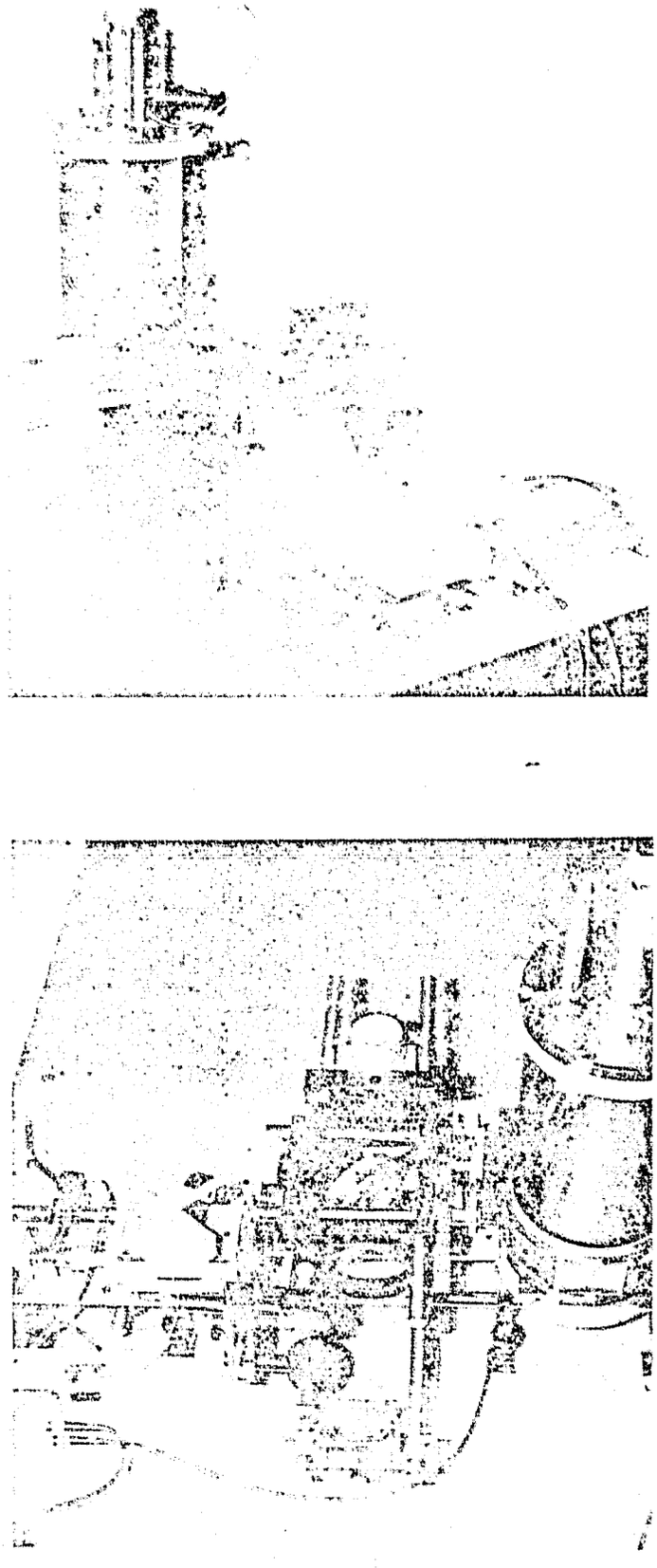

Figure 40: Laboratory version of the feed monitor system

bundle has to be converted into a parallel bundle of about 3 mm diameter. In order to do this, a Germanium lens (focal length f = 11 mm, diameter of aperture : 4 mm).was installed in the laser dewar at a distance of 11 mm from the crystal, whose transmission at 4.4 μm wavelength is 0.7 ± 0.1. From the spatial intensity distribution of the laser (see Figure 22 a, p. 40) and the described geometric relationships of the figure, the utilized fraction of laser energy is about 50% (that is, about 25 W). In addition, the diameter of the collimitered beam bundle was determined as a function of the distance to the laser (compare the scan method, section 4.1.4). The reference beam does have a diameter of more than 4 mm at a distance of 67 cm from the laser (maximum optical path of the radiation in the interferometer), however, the main fraction of intensity is concentrated within an appropriate circle. Approximately 40% of the intensity strikes the sensitive surface of the detector (diameter 2.25 mm). Figure 41 shows a horizontal and a vertical cross-section through the intensity distribution of the cross-sectional surface of the bundle at 9 cm and 67 cm distance. The properties of the studied laser bundle (intensity, divergence) permit its use in the feed monitoring system. /70

5.2 Tests of the Feed Monitoring System /71

Under consideration of the effectiveness of the beam splitter and the reflectivity of the cube corner (six reflections correspond to 75% transmission), together with the above losses caused by the geometry of the arrangement, we obtain a signal amplitude at the detector output in the range of 4 to 5 mV (see equation 3.14). This signal is amplified in a preamp (Infrared Laboratories Inc., Tucson, USA), whose input was adapted to the detector output, by a factor of 1,000 to 4 to 5 V, before it is evaluated in the positioning electronic system. The block diagram of the entire signal processing system is shown in Figure 42.

During the shift of the cube corner, the amplitude of the modulated signal changes by $\Delta S \leq 1V$. The larger fraction of variation consists in a monotonous component, caused by the small divergence of the beam bundle; the smaller fraction is defined by the periodic fluctuations and caused by the secondary lines appearing in the laser spectrum (Section 3.1). Figure 43 shows examples. The working point can be accurately adjusted during recording of the interferogram, since secondary lines are clearly noticed through the behavior of the amplitude, as we can see from the signal profile of the inaccurately adjusted working point (Figure 43 b).

One peculiarity of the laboratory setup is the noise sensitivity of the beam splitter, since the system is not operated in a vacuum. Noise like loud conversation excites the beam splitter to oscillations which initiate additional modulation and multiple pulses in the interferogram (Figure 44). Therefore, during tests all interfering noise had to be avoided. No effect of the soft motor noise on the interferogram was observed. /73

Only the error in feed monitoring for accurately adjusted working point will be discussed. The support point errors caused by the

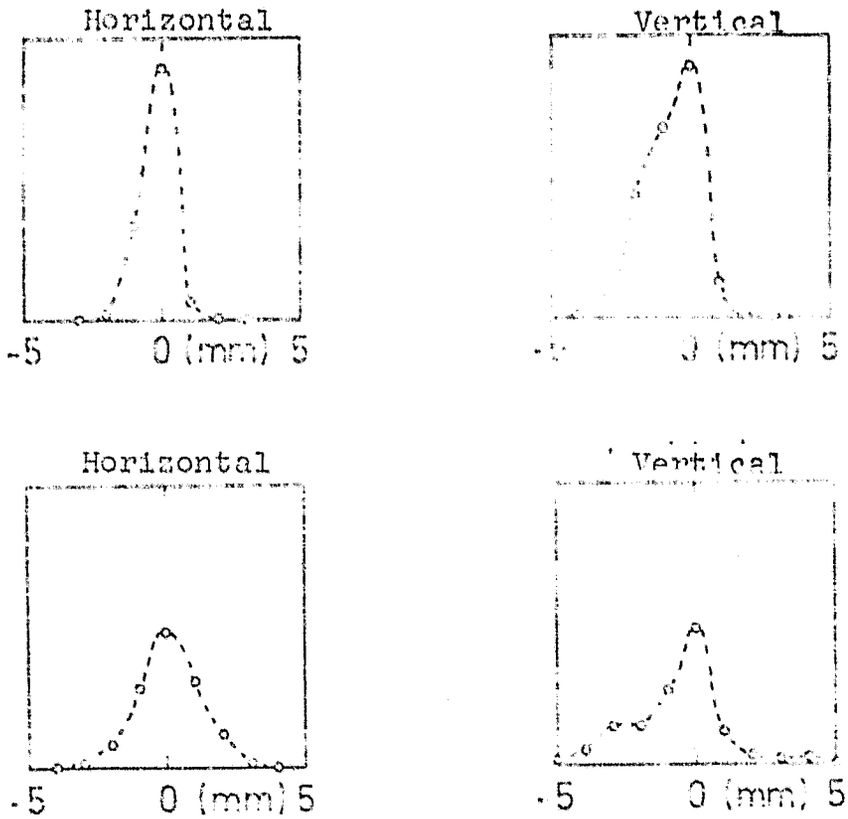

Figure 41: Relative intensity in the reference beam bundle plotted against horizontal and vertical local coordinates (perpendicular to beam direction) at a distance 9 cm (a) and 67 cm (b) from the laser. The local resolution is 1 mm by using a 1 mm perforated aperture in front of the InSb detector.

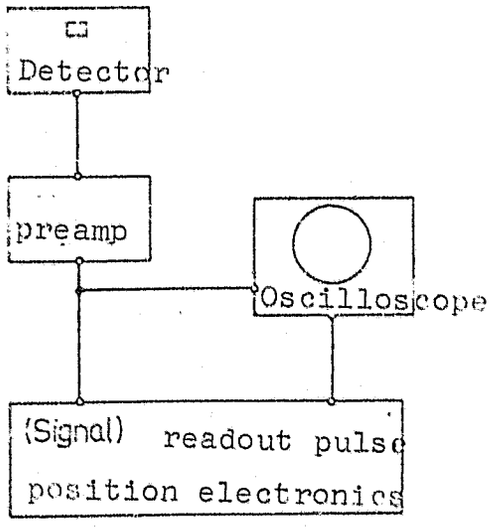

Figure 42: Block diagram of the electronic system to record and process the interferometer signal

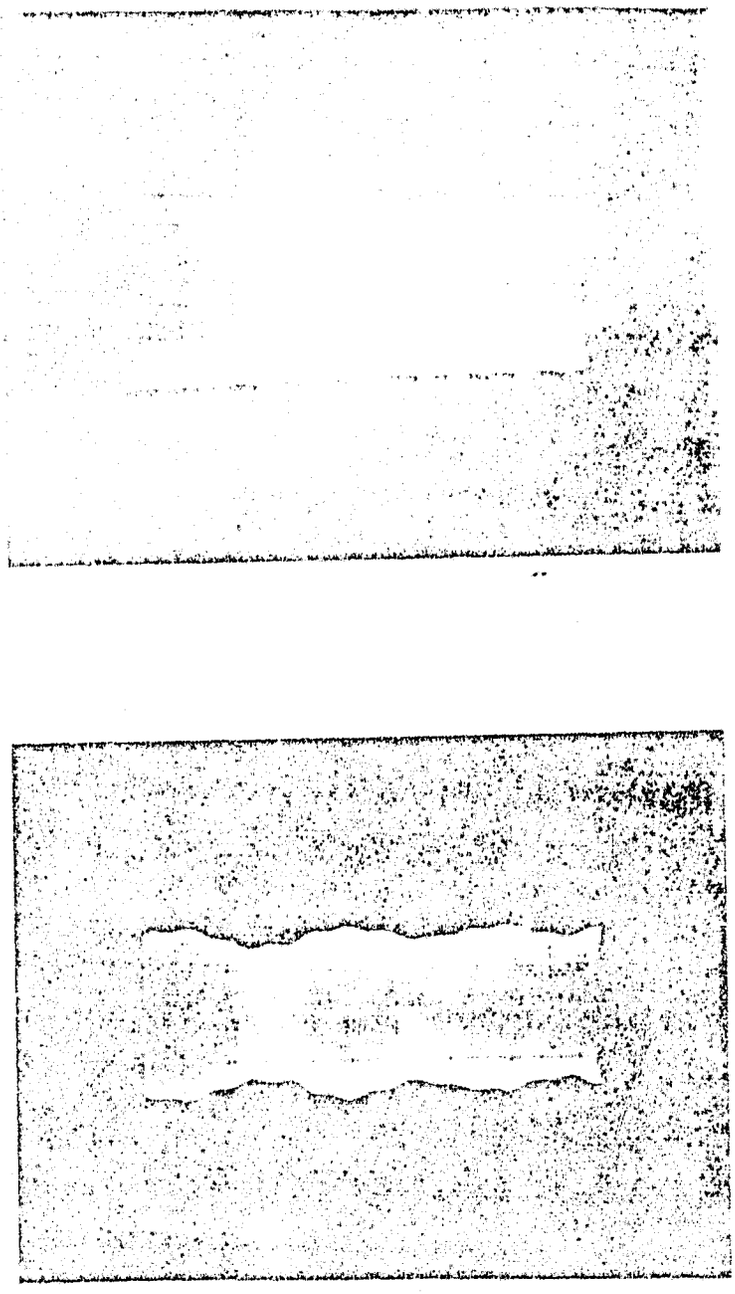

Figure 43: Profile of interferometer signal along an optic shift path of 1.8 cm.

a) operating the laser at the working point (0.959 A),

b) inaccurate adjustment of the working point. The behavior of the signal amplitudes can be seen by the chronological time change. From the periodic modulation, the relative intensity of secondary lines in the laser spectrum can be estimated.

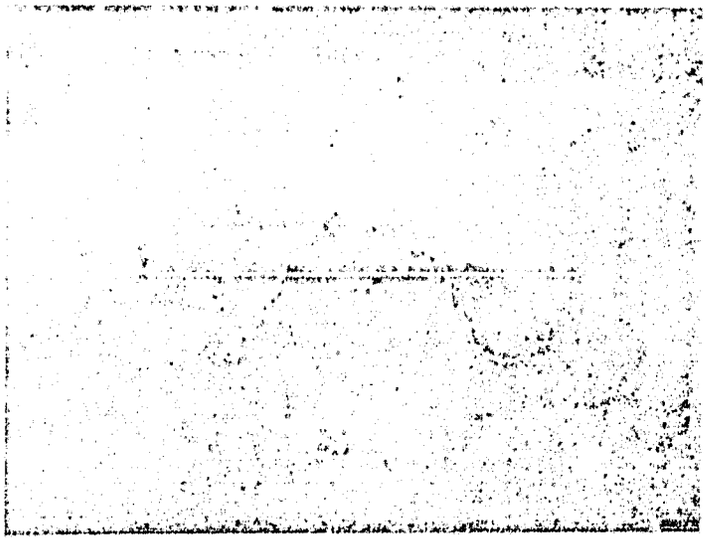

Figure 44: Interferometer signal for secondary noises with readout pulses given off by the position electronics at all points which can be considered as extreme positions or zero passages

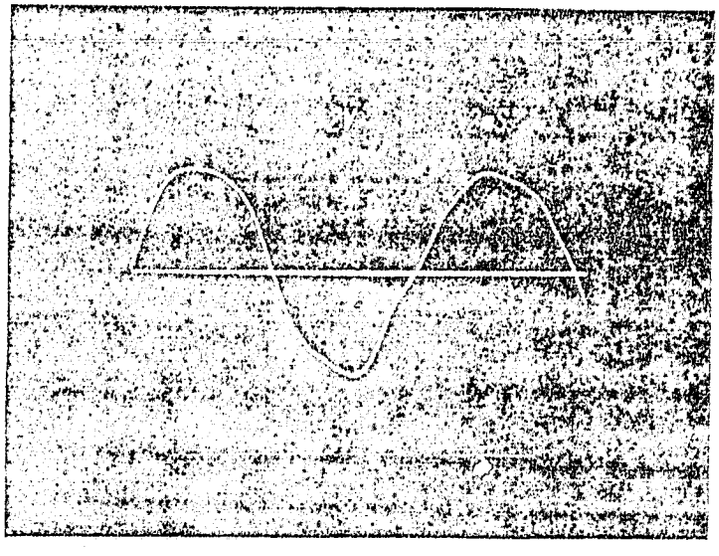

Figure 45: Inferometer signal with readout pulses. The deviations in readout pulses from the ideal support points are on the average less than 0.06 µm. The optical path shift between the pulses is 1.1 µm corresponding to a time difference of about 3 msec.

secondary lines are a maximum 0.03 μm according to equation 3.8, since they possess a fraction of only 5% of the main line intensity (ratio of intensities of secondary lines and primary lines $S_1/S_0 \approx 0.05$, see Figure 18 e, p. 35). Since the total noise voltage measured at the amplifier output of the operating system is still below 2 mV, the interferometer signal ($S = 4V$) has a S/N ratio of ≥ 2000. The resulting quadratic, averaged error of all support points remains limited to 0.03 μm (see Figure 39, p. 66). The maximum permissible value of 0.06 μm (see equation 3.6) is therefore clearly greater than the error obtained. Thus, all prerequisites for accurate work of the positioning electronic system and thus for a high resolution feed monitoring system have been created.

The shape of the interferometer signal deviates from an ideal sine curve since the actual feed velocity of the cube corner is not constant because of mechanical effects when moving the shift table. The interferometer signal was taken at various advance speeds and evaluated. Figure 45 shows the interferometer signal with the read pulses emitted by the positioning electronic system at an advance speed of $\approx$ 350 μm/sec, whereby a signal frequency of about 80 Hz resulted. The read pulses mark support points separated by 1.1 μm, even though the time in which the cube corner moves from one support point to the next is not constant. The support point errors resulting from the appearance of secondary lines in the laser spectrum and from the noise components of the signal amount to 0.06 μm (see above). Thus, a feed monitoring system has been constructed which meets the requirements outlined in Section 2.1. /74

Summary

For the helium cooled spectral, high resolution ($\frac{\nu}{\Delta\nu} \approx 10^4$) Michelson interferometer to be used aboard the German IR telescope GIRL on Spacelab, a new feed monitoring system was constructed as a laboratory model and tested successfully. This model is a position interferometer which uses the beam path of the GIRL interferometer and a monochromatic IR emission source and a suitable detector. As emission source, for the first time a semiconductor diode laser with a wavelength of 5 μm was used and is arranged like the detector in the GIRL cryostat (high vacuum, temperature $T < 10K$).

The significant fraction of the work consisted in deriving the critical properties of the component (diode laser, detector, beam splitter) critical for the system and to test them experimentally. Accordingly, for a used emission power of the laser of 25 μW with a sensitive detector (measured NEP $\approx 10^{-12}$ W/$\sqrt{\text{Hz}}$), interferograms were taken from which the positioning values were determined by scanning by a computing read electronic system.

The test results of the used component show that the feed monitoring performed exhibits the required accuracy of 0.06 μm (for a dynamic range of 100 in the astronomic spectrum). Thus, the feed monitoring system of high resolution has been constructed which is suitable for use on satellites in cryogenic conditions.

REFERENCES

1. M. Born, E. Wolf, "Principles of Optics", Pergamon Press, London, 1959

2. J. M. Dowling, "Double-Beaming in Fourier Spectroscopy", Aspen INternational Conference on Fourier Spectroscopy 1970, p. 55, AFCRL-71-0019

3. Du Pont de Nemours (Deutschland) GmbH Duesseldorf: Mylar--Optical Properties (techical information), 1979.

4. D.N.B. Hall, R.S. Aikens, R. Joyce, T.W. McCurnin, "Noise Limited Operation of Photovoltaic InSb-Detectors", Appl. Optics, 14, p. 450, 1975

5. R. D. Hempstead, M. Lax, "Classical Noise VI. Noise in Self-Sustained Oscillators near Threshold", Phys. Rev., 161, p. 350, 1967

6. E.D. Hinkley, C. Freed, "Direct Observation of the Lorentzian Line Shape as Limited by Quatum Phase Noise in a Laser above Threshold", Phys. Rev. Lett. 26, no. 6, p. 277, 1969

7. R. D. Hudson, J.W. Hudson, "Infrared Detectors, Benchmark Papers in Optics 2", Dowden, Hutchinson & Ross, Inc., Stroudsburg, 1975

8. R. Katterloher, "A Bolometer for 0.3 Kelvin", Dissertation, MPI-PAE/Extraterr. 143, 1978

9. H. Kressel, "Semiconductor Lasers", in: Levine, De Maria, Lasers 3, Marcel Dekker Inc., New York, 1971

10. D. Lemke, G. Klipping, M. Grewing, H. Trinks, S. Drapatz, K. Proetel, "GIRL - A Liquid Helium-Cooled Infrared Observatory for Space-lab", SPIE, Electro-Optical Technical Symp. & Workshop, Huntsville, 1979

11. M.I. Nathan, "Semiconductor Lasers", Proc. IEEE, 54, 1966

12. D.A. Naylor, R.T. Boreiko, T.A. Clark, "Mylar Beam-Splitter Efficiency in Far Infrared Interferometers: Angle of Incidence and Absorption Effects", Appl. Optics, 17, p. 1055, 1978

13. T.L. Paoli, J.E. Ripper, T.H. Zachos, "Resonant Modes of GaAs Junction Lasers 2. High-Injection Level, "IEEE J. Quantum Electronics 5, No. 6, p. 271, 1969

14. H.E. Parsche, "A Laser Controlled Fourier interferometer for the visible spectral range", Dissertation, Technical University of Munich, 1973

15. H. Rieck, "Semiconductor Laser, G. Braun, Karlsruhe, 1968

16. H. Sakai, "Consideration of the Signal-To-Noise Ratio in Fourierspectroscopy", Aspen Internat. Conf. on Fourier Spectroscopy 1970, p. 19, AFCRL-71-0019

17. D.R. Smith, E.V. Loewenstein, "Optical Constants of Far Infrared Materials. 3: Plastics", Appl. Optics, 14, p. 1335, 1975

18. G.A. Vanasse, H. Sakai, "Fourier Spectroscopy" in: Wolf, Progress in Optics 6, p. 261, North Holland Publ. Comp., Amsterdam, 1971

19. R. Wilsczek, personal conversation, 1979.

Appendix 1

/78

Noise in the Fourier spectrum for random (statistic) read error.

Let the support point errors Δx at the ideal support points x_n assume the statistic values Δx_n, $n = 1,\ldots,N_o$; N_o: number of support points. At distance 1 we have the following equation for the support points:

$$[illegible] \qquad (A.1)$$

Along the interval $0 \leq x \leq L$, a stepwise, constant (stepping) function $f(x)$ is defined which assumes the value of the support point error at the support point:

$$f(x) := \Delta x_n \quad \text{for } x_n \leq x < x_{n+1},\ n = 1,\ldots,N_o.$$

The function $f(x)$ is limited along the given interval and is stepwise constant. The Fourier series $F(x)$ of the function:

$$F(x) = \frac{a_o}{2} + \sum_{m=1}^{M} \left(a_m \cos m\frac{2\pi}{L}x + b_m \sin m\frac{2\pi}{L}x\right)$$

therefore converges on the average to $f(x)$. Since the number of different values x_n at the discreet support points x_n is at most equal to N_o, the series development is terminated at $m = N_o$. From the convergence at the mean we obtain the equation:

$$\frac{2}{L}\int_0^L (f(x))^2 dx \geq \frac{a_o^2}{2} + \sum_{m=1}^{N_o} (a_m^2 + b_m^2) \qquad (A.2)$$

The Fourier coefficients a_m and b_m represent the amplitudes of the periodic error components generating the ghost line pairs in the Fourier spectrum. As an average square of the amplitude a^2 we define:

$$\overline{a^2} := \frac{1}{2N_o} \sum_{m=1}^{N_o} (a_m^2 + b_m^2)$$

With equation A.2 we obtain, by neglecting a_o (the constant term does not result in ghost lines):

$$\overline{a^2} = \frac{1}{2N_o}\frac{2}{L}\int_0^L (f(x))^2 dx = \frac{1}{N_o L}\sum_{m=1}^{N_o} \Delta x_m^2 \cdot 1$$

From this results the following equation, after application of the standard deviation of the support points: /79

$$[illegible] = \frac{1}{[illegible]} \sum_{m=1}^{N_o} \Delta x_m^2$$

After application of equation A.1, the relationship between the quadratic averaged error amplitude and the quadratic averaged support point error is determined:

$$\overline{a^2} = \frac{1}{N_o} \sigma_x^2 \qquad (A.3)$$

The periodic support point error of amplitude "a" generates a pair of ghost lines in the Fourier spectrum with relative line peaks

$$\beta_1 = \pi \tilde{\nu}_F a$$

in the vicinity of a real spectral line (wave number ν_F; see Section 2.1). The different components of the statistic support point error generate ghost lines in the vicinity of a spectral line in all spectral elements of the Fourier spectrum. According to equation 2.3, for the average quadratic relative amplitude of the ghost lines for the presence of a spectral line we have:

$$\overline{\beta_1^2} = (\pi \tilde{\nu}_F)^2 \overline{a^2}$$

and with equation A.3 we have (in the worst case):

$$\overline{\beta_1^2} = (\pi \tilde{\nu}_F)^2 \frac{1}{N_o} \sigma_x^2 \qquad (A.4)$$

The number of independent spectral elements is N_o (see Section 1.3, equation 1.2, 1.3). The ghost lines appearing in all spectral elements attributable to the presence of a genuine spectral line represent noise in the Fourier spectrum. Additional genuine spectral lines provide additional contributions to spectral noise through the attendant ghost lines. At a maximum of N_o spectral lines of the same intensity, for the relative ghost line amplitude we have the following equation, averaged quadratically over the spectral elements:

$$\overline{\beta} = \sqrt{\overline{\beta_1^2}} \cdot \sqrt{N_o} \quad .$$

$\overline{\beta}$ represents the average noise at each spectral element of the Fourier spectrum, related to an average line intensity. With equation A.4 the relation to the standard deviation of the support points is obtained:

$$\overline{\beta} = \pi \tilde{\nu}_F \sigma_x$$

Appendix 2

/80

Description of the Positioning Electronic System

The positioning electronic system is illustrated in Figure 46. An input signal whose freqency f lies in the capture range (50 - 130 Hz with regard to the intended signal frequency 90 Hz), effects the tuning of the pulse generator to 128f, whereby the integration time is specified as $\tau = T/128$ (T: period of the interferometer signal, see Section 2.2). Below, the profile of the interferometer signal will be described by the electronics.

The input voltage is digitalized in increments of u = 2.44 mV = $U_o/2048$. U_o is the maximum input voltage which may not be exceeded by the signal amplitude in order that the support points can be properly evaluated. A relative extreme is found if we change the sign of the difference from the actual measured value (memory 1) and the measured value taken one time interval ago (memory 2), and the attendant value (in comparator 1) is stored. From the maximum value (memory 3) and the subsequent minimum value (memory 4), the arithmetic average is calculated. The comparators 3 and 4 prevent use of a secondary maximum or minimum. The result serves as a precalculated zero line for the following zero passages. The zero passage is recognized upon change in sign of the different from the actual measured value and this average value (in comparator 2). According to the named change in sign at the comparators 1 and 2, the release of a read pulse is triggered.

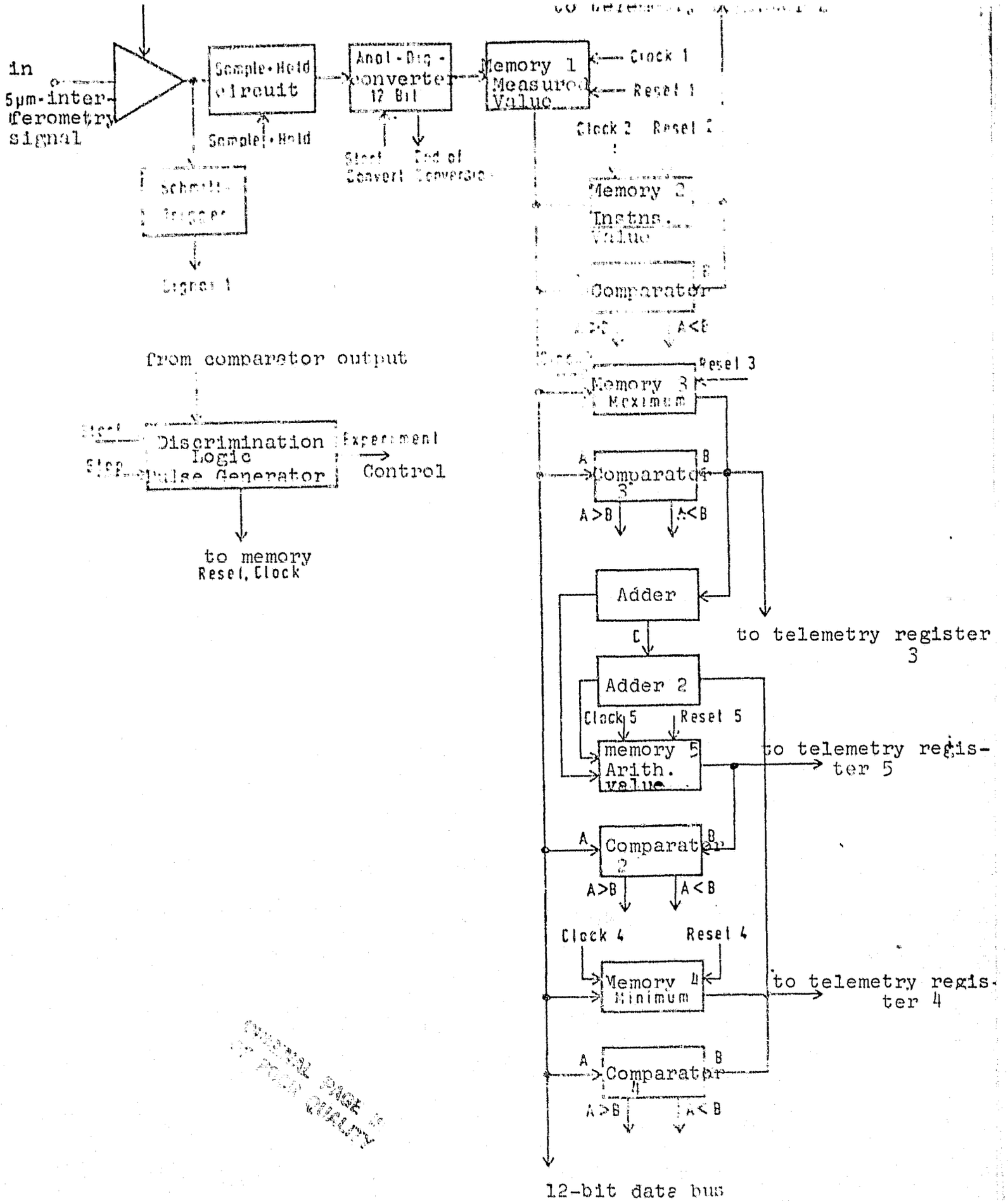

Figure 46: Block diagram of the position electronic system

Appendix 3

/82

Position of the zero passages in the interferogram of a Lorentz line

The interferogram of a Lorentz line has the form (equation 3.2):

$$I(x) = 1 + \exp(-2\pi\varepsilon x) \cdot \cos(2\pi\tilde{\nu}_L x) \qquad (A.5)$$

Because of the very small shift in extremal positions of I(x) (see Equation 3.4), at the known line width $\varepsilon = \ldots$ the following equations approximately apply to the value of a maximum and the subsequent minimum:

$$I_{max} = 1 + \exp(-\pi\varepsilon\lambda_L n)$$

$$I_{min} = 1 - \exp(-\pi\varepsilon\lambda_L (n+1)), \quad n \in \mathbb{N}$$

The arithmetic average M_o thus is:

$$M_o = \frac{1}{2}(I_{max} + I_{min}) = 1 + \frac{1}{2}\exp(-\pi\varepsilon\lambda_L n)\cdot(1 - \exp(-\pi\varepsilon\lambda_L)) \qquad (a.6)$$

In the feed monitoring system, this arithmetic average value is used as a zero line; it is different from the ideal value I = 1 ($M_o > 1$). Thus, a shift in position of the zero passage recognized by the feed monitoring system to the ideal position of the zero position results. This shift Δx is now calculated.

For the position of the zero points of I(x) we have:

$$x_n = (n + \frac{1}{2})\frac{\lambda_L}{2} \quad , \quad n \in \mathbb{N} .$$

The position of the two zero passages used in the feed monitoring system at $x_n = (n + \frac{3}{2})\frac{\lambda_L}{2}$ and $x_n = (n + \frac{5}{2})\frac{\lambda_L}{2}$ result through equating equation A.5 and A.6. For the zero passage with the greatest deviation $(x_n' = (n + \frac{5}{2})\frac{\lambda_L}{2} + \Delta x)$ we have:

$$\exp(-\pi\varepsilon\lambda_L\cdot(n + \frac{5}{2}) - 2\pi\varepsilon\Delta x)\cdot\cos(\pi(n + \frac{5}{2}) + 2\pi\tilde{\nu}_L\Delta x) =$$

$$= \frac{1}{2}\exp(-\pi\varepsilon\lambda_L n)\cdot(1 - \exp(-\pi\varepsilon\lambda_L))$$

From this follows with $\varepsilon\Delta x \ll 1$

$$\sin(2\pi\tilde{\nu}_L\Delta x) = \frac{1}{2}(-1)^n\exp(\frac{5}{2}\pi\varepsilon\lambda_L)\cdot(1 - \exp(-\pi\varepsilon\lambda_L)),$$

and for small deviations $(\frac{\Delta x}{\lambda_L} \ll 1)$ and small line widths $\frac{\varepsilon}{\ldots} \ll$ there results:

$$\Delta x = \frac{1}{4}(-1)^n \frac{\varepsilon}{\tilde{\nu}_L^2} .$$

Appendix 4

/83

Position of the zero points in the interferogram of two spectral lines

The interferometer signal disturbed by a secondary line of the laser can be written in the following form (index L = main laser line, indix N = secondary line, see Equation 3.6):

$$S(x) = S_0 \sin(2\pi \tilde{\nu}_L x) + S_1 \sin(2\pi \tilde{\nu}_N x) \qquad (A.7)$$

The zero points of the undisturbed signal S_L

$$S_L(x) = S_0 \sin(2\pi \tilde{\nu}_L x)$$

lie at $x_n = n \frac{\lambda_L}{2}$. . For the zero points x_n' of S(x) we now use:

$$x_n' = n \frac{\lambda_L}{2} + \qquad (A.8)$$

and substitute into S(x) = 0 (equation A.7). With the approximation for small shifts $\left(\frac{\Delta x}{\lambda_L} \ll 1, \frac{\Delta x}{\lambda_N} \ll 1\right)$ we have:

$$0 = S_0 (-1)^n 2\pi \tilde{\nu}_L \Delta x + S_1 (\sin(2\pi \tilde{\nu}_N x_n) + 2\pi \tilde{\nu}_N \Delta x \cdot \cos(2\pi \tilde{\nu}_N x_n))$$

Thus, for the shift Δx of the zero points of S(x) compared to the ideal position we have:

$$\Delta x = \frac{-\frac{S_1}{S_0} \sin(2\pi \tilde{\nu}_N x_n)}{(-1)^n 2\pi \tilde{\nu}_L + \frac{S_1}{S_0} \cdot 2\pi \tilde{\nu}_N \cdot \cos(2\pi \tilde{\nu}_N x_n)}$$

Now, with the approximation for small intensity ratios of the main and secondary line $(S_1/S_0 \ll 1)$, we have: /84

$$\Delta x = \frac{\frac{S_1}{S_0} (-1)^{n+1} \sin(2\pi \tilde{\nu}_N x_n)}{2\pi \tilde{\nu}_L} \qquad (A.9)$$

because

$$\sin(2\pi(\tilde{\nu}_L - \tilde{\nu}_N)x_n) = \sin(2\pi \tilde{\nu}_L x_n)\cos(2\pi \tilde{\nu}_N x_n) - \cos(2\pi \tilde{\nu}_L x_n) \cdot \sin(2\pi \tilde{\nu}_N x_n)$$

$$= (-1)^{n+1} \sin(2\pi \tilde{\nu}_N x_n)$$

there follows from equation A.9 by use of $\Delta\tilde{\nu} = |\tilde{\nu}_N - \tilde{\nu}_L|$

$$\Delta x = \frac{\lambda_L}{2\pi} \frac{S_1}{S_0} \sin(2\pi \Delta\tilde{\nu} x_n) \qquad (A.10)$$

The maximum shift Δx_{max} occurs when a zero point x_n' of $S(x)$ coincides with an extremum of the interference $S_N(x)$. Then from equation A.7 and A.8 we have:

$$0 = S_o(-1)^n \sin(2\pi \tilde{\nu}_L \Delta x_{max}) \pm S_1$$

Thus, we obtain an error amplitude $a = |\Delta x_{max}|$

$$a = \frac{\lambda_L}{2\pi} \arcsin \frac{S_1}{S_o} \quad ,$$

That is, for $S_1/S_o \ll 1$ the amplitude of Δx is, as in equation A.10:

$$a = \frac{\lambda_L}{2\pi} \frac{S_1}{S_o} \quad .$$

Acknowledgement

I wish to thank Dr. J. Truemper and Dr. G. Haerendel for the opportunity to perform this work at the Institute for Extraterrestrial Physics.

My special gratitude is due Dr. S. Drapatz and Dr. R. Hofmann for many valuable technical suggestions and discussions on the management and overview of the project.

Dr. R. Katterloher and D. Zasche provided much valuable stimulus in the implementation of the project.

For their friendly support and advice in questions of the position electronic system I wish to thank Mr. G. Saemann who constructed this electronic system.

Mr. A. Fritsch and Mr. A. Strauss helped with the practical work.

The workshop of the Institute is owed a debt of gratitude for the reliable fabrication of numerous components.

I certify that I have prepared the present project independently and without outside help.

February 1980.